Design and Implementation of Microwave Bandpass Filters Based on CRLH-TL and Interdigital Ring Resonators

Li Zhu

A Thesis

in

the Department

of

Electrical and Computer Engineering

Presented in Partial Fulfillment of the Requirements

for the Degree of Master of Applied Science (Electrical and Computer Engineering) at

Concordia University

Montreal, Quebec, Canada

April 2008

Your file Votre référence
ISBN: 978-0-494-40901-5
Our file Notre référence
ISBN: 978-0-494-40901-5

ABSTRACT

Design and Implementation of Microwave Bandpass Filters Based on CRLH-TL and Interdigital Ring Resonators

Li Zhu

Microwave printed filters are preferred in modern mobile and satellite communication systems due to low cost, compact size, and high accuracy. In order to facilitate circuit integration and achieve high information capacity in a communication system, volume miniaturization and bandwidth modulation of the filters becomes critical. Such requirements make design and implementation of filters extremely challenging. Hence, the work presented in this thesis is focused on two aspects, namely, compact printed filter design and effective bandwidth modulation techniques.

First, a simple composite right/left handed (CRLH) transmission line (TL) structure is proposed. Based on this structure, a bandpass filter which offers several advantages (*e.g.* compact size and low loss over traditional filters) is designed. A CAD algorithm for automated CRLH filter design is also implemented, and demonstrated through a practical example. Second, a set of ring filters with adjustable bandwidths are proposed. These filters are implemented by a combination of hairpin resonators, interdigital capacitors and/or etched slots, leading to considerably wider bandwidths as compared to traditional ring filters. In addition, by changing the geometrical parameters of the interdigital capacitors and etched slots, the bandwidth can be easily adjusted for different applications. The filters feature two transmission zeros, whose locations can be accurately determined by means of the semi-analytical model developed as part of this

thesis. The proposed filter units can be cascaded to obtain sharper cutoff frequency responses. Several these filters have been fabricated and tested using Anritsu 37369D vector network analyzer. The frequency responses from measurements are in good agreement with those from simulations in the 5-9 GHz range.

Acknowledgements

First of all, I would like to express my sincere appreciation for my research advisors, Dr. Vijay Devabhaktuni and Dr. Chunyan Wang, for their guidance and support over the two years' journey. I would like to thank them for bringing me into the CAD modeling and design group at Concordia, where I have been able to work in my favorite microwave field. Inspirations drawn from the fruitful and enlightening technical discussions with them have helped me overcome difficulties encountered in the design and experiments and have been crucial in making these projects successful. I am especially grateful for their constant encouragement, which will continue to promote my desire to do my best in my future career.

I would also like to express appreciation for the expert advice and counsel of Dr. Don Davis (Part-time faculty of ECE department of Concordia), Dr. Ming Yu (Director and senior RF/microwave engineer of COM DEV) and Mr. Jules Gauthier (Senior RF/microwave engineer of Advanced Research Centre in Microwaves and Space Electronics at Ecole Polytechnique de Montreal). Their valuable suggestions as well as support in providing test equipments have appreciably accelerated the progress of my research projects.

I feel very lucky to have worked with the current and previous members of Concordia CAD modeling and design group, Navid Arbabi, Arash Kashi, Niladri Roy, Kaustubha Mendhurwar, Farzin Manoucheri, Mani Najmabadi, Rajasekhar Kakumani, Joshua Frankel and Ahmad Zbeeb, each of whom gave me a lot of help in many aspects and made my time at Concordia enjoyable.

Lastly I'd like to extend my heartfelt appreciation to my girlfriend, Yang Tang and my parents, Zhenmin Zhu and Ping Huang, whose ongoing guidance, support, and understanding gave me the strength to finish this work.

To my loving parents
Zhenmin & Ping

Table of Contents

List of Figures

List of Tables

List of Symbols and Abbreviations

A_{max}	maximum pass-band attenuation
A_{min}	minimum stop-band attenuation
B	magnetic flux density
BW	bandwidth
B_{ij}	susceptance
C'	*per-unit-length* capacitance
C	self-capacitance
C_{int}	capacitance of interdigital capacitor
C_m	mutual capacitance
CAD	computer aided design
CRLH	composite right/left handed
D	arm length of interdigital capacitor
E	electric field intensity
EM	electromagnetic
f_0	central frequency
f_{r1}	lower resonant frequency
f_{r2}	higher resonant frequency
FBW	fractional bandwidth
G'	*per-unit-length* conductance
J	susceptance
k	wave number
K	coupling coefficient

L'	*Per-unit-length* inductance
LH	left-handed
LHM	left-handed materials
L_m	mutual inductance
M	width of fingers
MMIC	Monolithic Microwave Integrated Circuit
N	number of fingers
NC	negligible change
P	port
Q_E	external quality-factor
Q_u	unloaded quality factor
RH	right-handed
R'	*per-unit-length* resistance
TL	transmission line
SRR	split-ring resonator
SHF	super high frequency
S_{int}	coupling gap
UCLA	University of California, Los Angeles
UCSD	University of California, San Diego
V_p	phase velocity
V_g	group velocity
X_f	error term
Y_0	characteristic admittance
Z_0	characteristic impedance

z_c	impedance of interdigital capacitor
β	phase constant
μ	permeability
ε	permittivity
Δl	additional microstrip length of interdigital capacitor

Chapter 1

Introduction

The term *microwave* refers to the frequency range from 300 MHz to 300 GHz, with corresponding electrical wavelengths from 1 m to 1 mm. Microwave components are often distributed elements, where the phase of a voltage or current changes significantly over the physical extent of the device. Even though microwave engineering had its beginning in the early 20th century, significant developments in high frequency solid-state devices, microwave integrated circuits, and the ever-increasing applications of modern microsystems have kept the field active and vibrant. The majority of today's microwave technology applications are in communication systems, radar systems, medical systems and environmental remote sensing [1]-[3]. The most ubiquitous use of microwave technology is in cell phone systems. By 1997, there were more than 2 billion cellular subscribers worldwide. Satellite systems, such as Global Positioning Satellite (GPS) system and Direct Broadcast Satellite (DBS) system, have been extremely successful in providing cellular, video, and data connections worldwide. The advantages

offered by microwave systems, including wide bandwidths and line-of-sight propagation, have proved to be critical for both terrestrial and satellite communications systems and have thus provided an impetus for the continued development of low-cost miniaturized microwave components. In the whole microwave spectrum, the super high frequency (SUF) band that is from 3 GHz to 30 GHz, is widely utilized in military satellite system.

In most microwave communication systems, filters play extremely important role. Microwaves filters separate or combine different frequencies and are used to select or confine the microwave signals within assigned spectral limits. Emerging applications such as wireless communications continue to challenge microwave filter designers with ever more stringent requirements: higher performance, smaller size, etc. In the following sub-sections, basic characteristics and existing implement method of microwave filters will be introduced, and motivation, objective and scope of the thesis will be presented.

1.1 Microwave Filter

A microwave filter is a two-port network used to control the frequency response at a certain point in a microwave system by providing transmission at frequencies within the passband and attenuation in the stopband. Typical frequency responses include lowpass, highpass, bandpass, and bandstop characteristics. Microwave filter applications can be found in virtually any type of microwave communication, radar, or test and measurement system. The fundamental use of filters in electrical engineering is to shape signal spectrum, which is especially crucial in reducing input signal noise in receivers and spurious emissions in transmitters. In electrical engineering, filtering can be intentional,

as in the input stage of a receiver, or unintentional, as in the transmission path of a microwave signal. It is important to understand that almost every physical system has some sort of filtering action built in whenever a signal, an input, an output, and a transmission path can be defined in the system.

Microwave passive filters have traditionally been built using waveguides and coaxial lines. Recent microwave printed filters have unique advantages over waveguide and coaxial filters in terms of low cost, repeatability, high accuracy, and compact size. Another advantage of printed filters is their easy integration with active circuits (*i.e.*, filters can be fabricated on the same substrate with transistor amplifiers, oscillators, and other active circuits). Today, microstrip lines are perhaps the most common materials for microwave printed circuits, because of their simplicity, ease of manufacturing and high suitability for incorporation with active devices. Recent advances in materials and fabrication technologies, including metamaterials, monolithic microwave integrated circuit (MMIC), microelectromechanic system (MEMS) have stimulated research on novel microstrip filters.

In the past decade, metamaterials with simultaneous negative permittivity (ε) and permeability (μ), more commonly referred to as left-handed materials (LHM), have received substantial attention in the scientific and engineering communities. *Science* magazine even named LHMs as one of the top ten scientific breakthroughs of 2003 [4]-[6]. Experimental verification of LHMs did not occur until three decades later by a group at University of California, San Diego (UCSD). The UCSD's LHM consisted of copper split-ring resonators (SRRs) and thin copper wires, providing negative permeability and

negative permittivity, respectively [7]. Soon, several researchers realized artificial LHMs by Transmission Line (TL) approach [8][9]. The TL approach of LHMs led to several microwave resonant structures with low insertion loss and wide bandwidth.

During the same period, advances in computer aided design (CAD) tools such as full-wave electromagnetic (EM) simulators have revolutionized filter design [10]. In the past few decades, CAD of microwave components has greatly progressed due to an increase in the overall design complexity of modern satellite communication systems. Currently, a plethora of CAD tools, *e.g.* Ansoft's *HFSS*, Zeland's *IE3D*, Agilent's *ADS*, etc., are available for microwave designers. These tools not only help in the design of a microwave circuit, but also facilitate optimization of the circuit for improved performance in terms of power, size, timing, etc. Many novel microwave filters with advanced filtering characteristics have been demonstrated in different CAD tools.

1.2 Motivation and Objectives

The recent and continuing evolution in telecommunications has implied stringent constraints on microwave systems and, especially on filters. Many applications and notably those involved in mobile and satellite communications, require to miniaturize the system dimensions without sacrificing electrical performances. The work presented in this thesis focuses on the desire to effectively reduce the volume and complexity involved in the design of printed microstrip bandpass filters, while keeping the same frequency response. Therefore, one of the objectives of the work is to implement a planar bandpass filter with relatively compacter size and lower loss than traditional planar bandpass filters,

and also to develop a CAD algorithm for automated design of the novel filters.

Apart from the volume of the circuit modules, the geometrical size of the microwave filter determines the filter's specifications such as bandwidth and loss. To extend the bandwidth of a microwave filter, the straight-forward approach is to reduce both its strip and slot widths, and a large number of line resonators are required in this case. However, such approaches may lead to a degradation of its filtering behaviors, *e.g.* quality factor, and also introduce some difficulties into the fabrication process due to its limitation of the strip/slot widths and conductor thickness/configuration. In order to overcome above challenge, it is desirable to implement wideband microwave filters without going beyond the fabrication limitation. Further, adjustable bandwidth of filters could offer excellent convenience for the microwave/RF system designers.

1.3 Scope and Organization

In order to achieve the objectives mentioned earlier, the work is divided into two phases, aiming volume minimization and bandwidth modulation. Scope of the research in the thesis includes:

- Designing a microstrip filter structure using the material whose resonance is independent of physical dimensions to achieve filter size minimization.
- Developing an effective CAD tool to facilitate automated design of this size-minimized filter.
- Designing a microstrip coupling structure that provides strong coupling strength.

- Implementing the bandpass filters with adjustable bandwidth based on the proposed coupling units.

The thesis is organized as follows:

Chapter 2 introduces basic coupling characteristics of LHM/LH-TL and microwave ring resonators, and presents some of the recent developments in terms of their design. Chapter 3 describes a proposed CRLH-TL filter with much smaller volume and lower loss than traditional printed filters. A new CAD algorithm for fully-automated design of CRLH filters is also presented in this chapter. Chapter 4 presents novel ring resonator filters with adjustable bandwidths and predictable transmission zeros. The fabrication and measurements are also discussed in this chapter. Chapter 5 draws conclusions and discusses possible contributions of this work leading to future research.

Chapter 2

Background

As mentioned before, microwave filters are traditionally built using waveguide [11] and coaxial lines [12]. However, following the enormous expansion in printed circuit technology and modeling techniques, more and more filters are currently implemented by printed circuits [13]-[15]. Printed filters have the advantages over rectangular or coaxial waveguide filters in terms of low cost, high accuracy and compact size. In addition, with the advances in full-wave EM simulation techniques, printed filters can be characterized accurately and rapidly. Perhaps the main disadvantage of regular printed filters is the high insertion loss associated due to mellaization and dielectric losses in some situations. For this reason, printed filters may not be suitable for applications where high power and very low loss are required.

Printed filters can be designed using microstrips, striplines and slotlines. Stepped-impedance, interdigital, and coupled-line filers are the most commonly used forms of printed filters [16]. In case of the stepped-impedance filters, the widths of the transmission lines are changed in a periodic manner to replicate series inductance and

shunt capacitance to implement filters. The interdigital filters consist of parallel arrays of quarter-wavelength transmission lines whose one ends are shorted to ground. For the coupled-line filter, cascaded sections of quarter-wavelength-long coupled transmission lines are used to design filters.

In the last decade, planer filters based on LH-TL and ring resonator structures have received increasing attention because of their unique properties and excellent performances. In the following sub-sections, the particular characteristics of these two typical structures and their applications are discussed.

2.1. LHM and LH-TL

In general, materials have two electromagnetic parameters, namely, permeability (μ) and permittivity (ε). μ is the degree of magnetization of a material that responds linearly to an applied magnetic field, while ε is a physical quantity describing how an electric field affects and is affected by a dielectric medium, thus relates to a material's ability to transmit an electric field. In essence, these two parameters determine how a given material interacts with EM radiation. A LHM is a material whose permeability and permittivity are both negative.

The basic characteristics of LHM can be analyzed by Helmholtz formulations:

$$\begin{cases} \nabla^2 \overline{E} + k^2 \overline{E} = 0 \\ \nabla^2 \overline{B} + k^2 \overline{B} = 0 \end{cases}, \tag{2.1}$$

where E is the electric field intensity (Volts/meter), B is the magnetic flux density (Tesla) and $k = \omega\sqrt{\mu\varepsilon}$ is the wave number, or propagation constant of the medium, its unit is 1/m. When $k^2 > 0$, Helmholtz formulation has a solutions, which means the wave can traverse the material. In nature, both ε and μ of material are positive, making $k^2 > 0$. Using Maxwell equations, we can derive the following equations:

$$\overline{k} \times \overline{E} = \omega\mu\overline{H}\,, \quad \overline{k} \times \overline{H} = -\omega\mu\overline{E}\,, \quad \overline{k} \cdot \overline{E} = 0\,, \quad \overline{k} \cdot \overline{H} = 0\,. \tag{2.2}$$

In (2.2), $\overline{k}$, $\overline{E}$ and $\overline{H}$ satisfy the RH triplet relationship, and the material satisfying such relationship is called RHM. Meanwhile, when both μ and ε are simultaneously negative, consequently $k^2 > 0$ still, the wave can also transmit in such material. However, in this case, $\overline{k}$, $\overline{E}$ and $\overline{H}$ satisfy LH triplet relationship instead of RH relationship. This kind of material is called LHM. Both RH and LH triplet relationships are shown in Fig. 2.1.

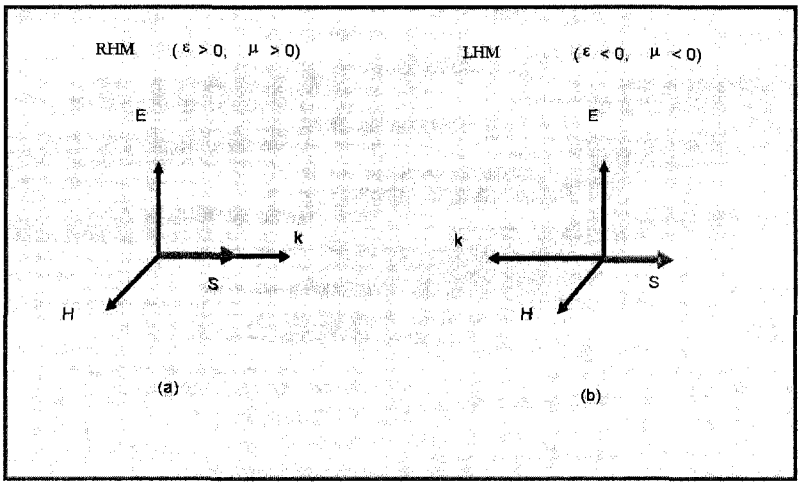

Fig. 2.1. RH triplet relationship of RHM and LH triplet relationship of LHM

LHMs have a wide range of applications in optical/microwave units, such as new types of modulators [17], bandpass filters [18], superlenses [19], and antennas [20]. However, the LH structures presented originally [6][7] were impractical for microwave applications, because of very lossy and narrow bandwidth characteristics. Alternative theories are desirable to gain a deeper insight into their behavior. In 2002, Prof. Tatsuo Itoh's group in UCLA introduced a transmission line (TL) approach of LH materials to realize an artificial lumped-element LH-TL and proposed a microstrip implementation of this line, which is a milestone for the development of the meta-materials [8]. Fig. 2.2 shows the layout and *S*-parameters of the artificial LH-TL.

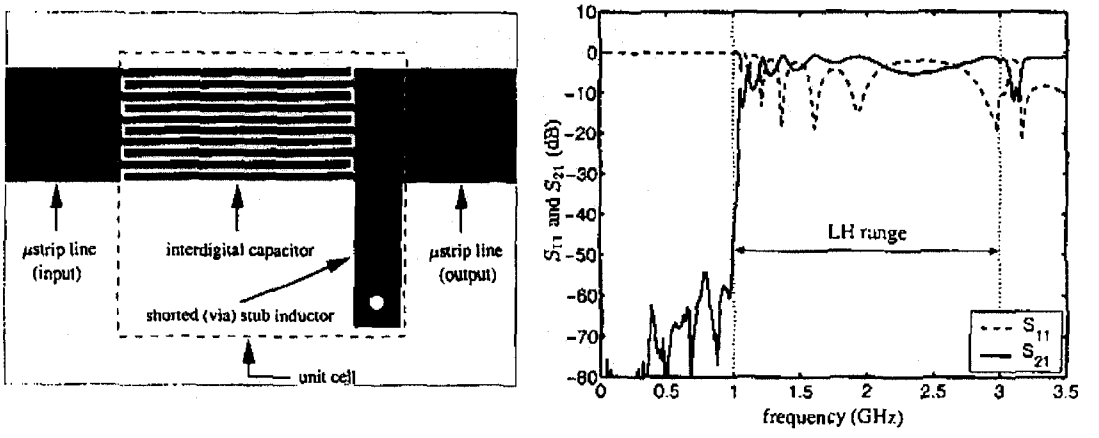

Fig. 2.2. The layout and *S*-parameters of the artificial LH-TL.

The comparisons of the basic microwave characteristics of LH-TL and RH-TL are summarized in the Table 2.1. The approach of LH-TL is based on the dual of the conventional RH-TL. The equivalent circuit of LH-TL is obtained by interchanging the inductance / capacitance and inverting the series/parallel arrangements in the equivalent

Table 2.1

Comparisons of basic microwave characteristics between LH-TL and RH-TL

	LH-TL	**RH-TL**
Equivalent Circuit (lossy)	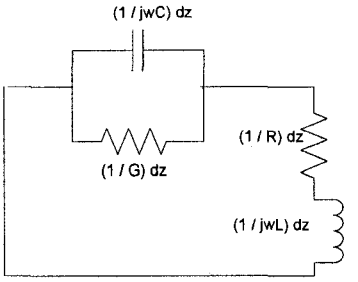	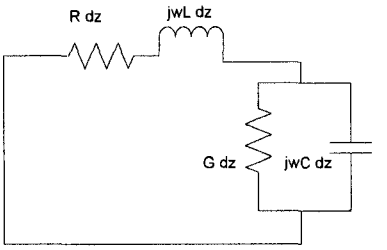
Equivalent Circuit (lossless)	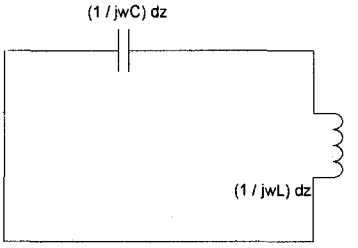	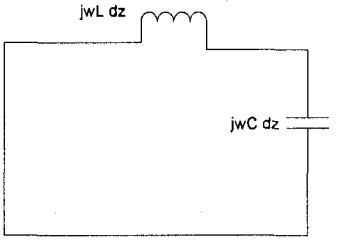
Propagation Constant	$\gamma(\omega)=\sqrt{Z'Y'}=\sqrt{(G'+j\omega C')^{-1}(R'+j\omega L')^{-1}}$	$\gamma(\omega)=\sqrt{Z'Y'}=\sqrt{(R+j\omega L)(G+j\omega C)}$
Phase Constant	$\beta(\omega)=-\frac{1}{\omega\sqrt{L'C'}}$	$\beta(\omega)=\omega\sqrt{LC}$
Phase and Group Velocities	$v_p=-\omega^2\sqrt{L'C'}$ $v_g=+\omega^2\sqrt{L'C'}$	$v_p=+(\sqrt{LC})^{-1}$ $v_g=+(\sqrt{LC})^{-1}$
Characteristic Impedance	$Z_0(\omega)=\sqrt{\frac{Z'}{Y'}}=\sqrt{\frac{(R'+j\omega L')}{(G'+j\omega C')}}$	$Z_0(\omega)=\sqrt{\frac{Z'}{Y'}}=\sqrt{\frac{(R+j\omega L)}{(G+j\omega C)}}$
Permittivity and Permeability	$\varepsilon(\omega)\propto-\frac{1}{\omega^2 L'}$ $\mu(\omega)\propto-\frac{1}{\omega^2 C'}$	$\varepsilon\propto L$ $\mu\propto C$

circuit of the RH-TL. Consequently, the LH-TL indicates a highpass nature, in contrast to the low-pass nature of the RH-TL.

The wave number γ of an LH-TL in terms of per-unit-length impedance $(Z' = Z/dz = (G' + j\omega C')^{-1})$ and admittance $(Y' = Y/dz = (R' + j\omega L')^{-1})$ is given by

$$\gamma(\omega) = \alpha(\omega) + j\beta(\omega) = \sqrt{Z'Y'} = \sqrt{(R' + j\omega L')^{-1}(G' + j\omega C')^{-1}}, \tag{2.3}$$

where R', L', C' and G' are *per-unit-length* quantities. For the lossless case, the propagation factor is given by

$$\beta(\omega) = -1/\omega\sqrt{L'C'}, \tag{2.4}$$

in which the negative sign indicates a negative phase velocity. The nonlinearity of β in (2.4) indicates frequency dispersion, with the antiparallel hyperbolic phase and group velocities:

$$\begin{aligned} V_p &= -\omega^2\sqrt{L'C'} \\ V_g &= +\omega^2\sqrt{L'C'} \end{aligned} \cdot \tag{2.5}$$

The characteristic impedance of the line is given by

$$Z_c(\omega) = \sqrt{Z'/Y'} = \sqrt{\frac{R' + j\omega L'}{G' + j\omega C'}}, \tag{2.6}$$

As can be summarized in Table 2.1, except the same expression of characteristic impedance, the LH-TL provides opposite nature to the RH-TL.

2.2. Existing LH Bandpass Filter

Based on the LH-TL structure of [8] and to meet the demand of MMIC for compactness, one unit of LH-TL was realized by cascading two inter-digital capacitors, which has been reported in [21]. As can be seen in Fig. 2.3(a), two out arms of each capacitor are grounded by vias, which are considered as arm-inductors. By adjusting the lengths of the arm-inductors and other parts of the inter-digital capacitor, a highpass frequency performance can be achieved. The dimensions of one unit of the improved structure and its equivalent *LC* circuit are shown in Fig. 2.3 (a) and Fig. 2.3 (b), respectively. Simulation results by Zeland's *IE3D* in Fig. 2.3 (c) illustrate high pass characteristics.

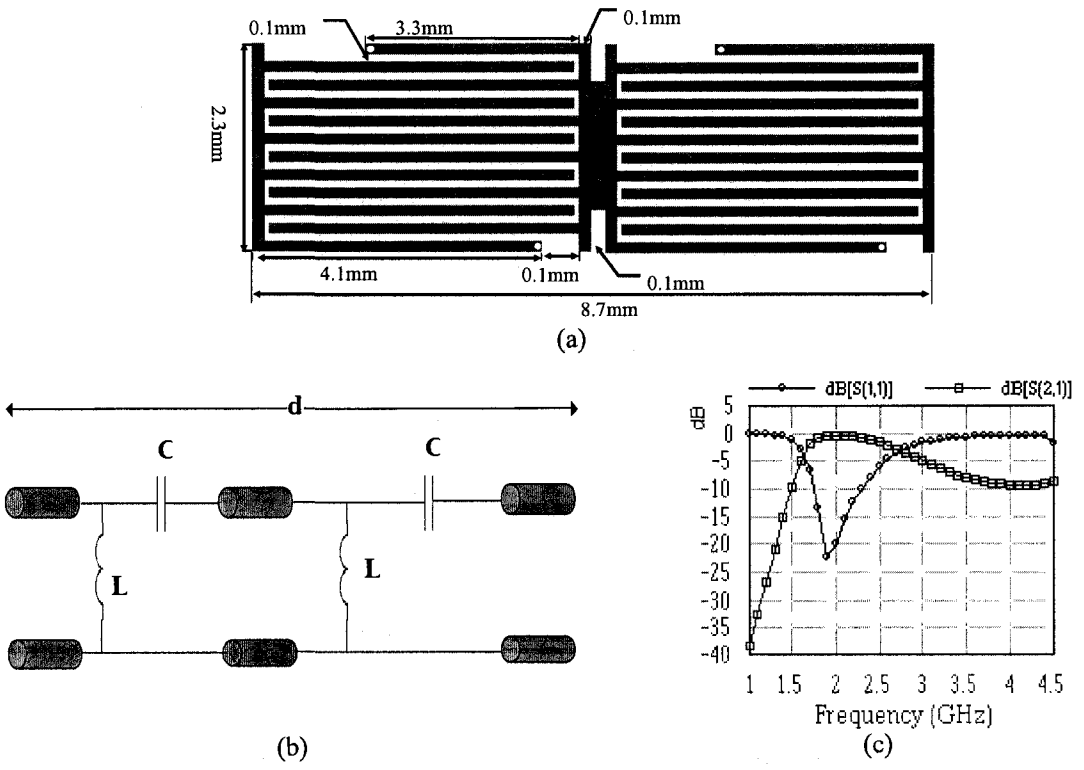

Fig. 2.3 (a) The layout of one unit, (b)the equivalent *LC* circuit and (c) the simulated *S*-parameters of an existing LH-TL structure. (ε_r = 9.8 and the substrate height is 0.38 mm)

As can be seen in Fig. 2.4(a), two such LH-TL units are coupled to implement a LH-TL bandpass filter. By means of odd and even mode analysis, the input impedance of the LH band-pass is determined to be

$$Z_{in} = \frac{1}{2\sin(\beta l)}\sqrt{(Z_{oe} - Z_{oo})^2 - (Z_{oe} + Z_{oo})^2 \cos^2(\beta l)}\,, \tag{2.7}$$

which is similar to that of traditional RH-TL band-pass filters [21]. According to (2.7), a resonation of the band-pass filter is obtained when $\beta l = \pm \pi/2$. Fig. 2.4 shows the layout and simulation result of the LH-TL bandpass filter. The LH-TL filter shows obvious bandpass characteristics with the center frequency at 2.5 GHz.

However, the structure is observed to have a limited bandwidth *i.e.* in the MHz range. If the specification of bandwidth were to be in the GHz range, this structure would not be suitable. Moreover, the coupling structure is relatively complicated which may cause additional expense in terms of fabrication.

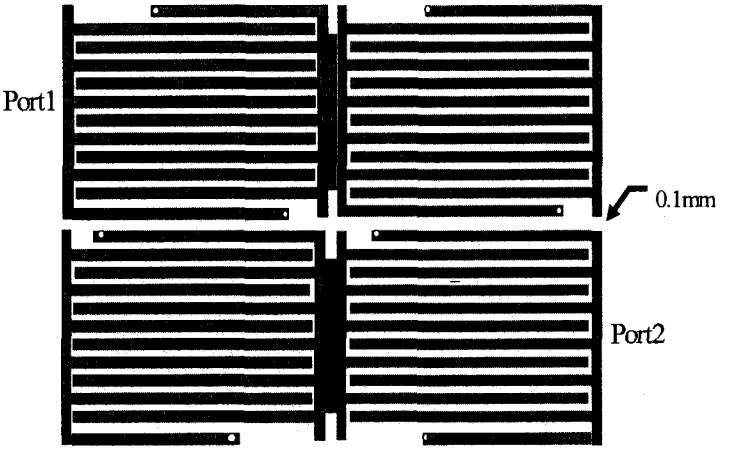

(a)

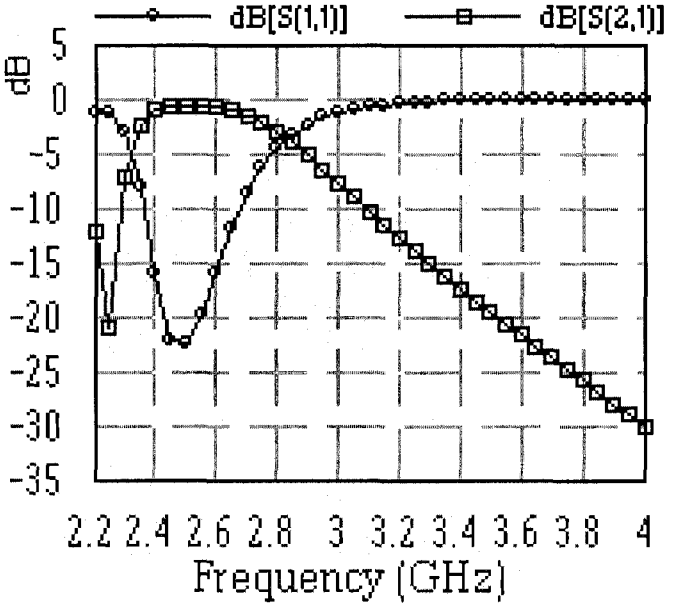

(b)

Fig. 2.4 (a) The layout and (b) the simulated *S*-parameters of an existing LH band-pass filter.

2.3. Microwave Ring Resonator

Microstrip ring structure was first proposed by P. Troughton in 1969 for the measurements of the phase velocity and dispersive characteristics of a microstrip line [22]. In the 1980s, applications using ring circuits as antennas, and frequency-selective surfaces emerged. Microwave circuits that use rings for filters, oscillators, mixers, baluns, and couplers [23]-[25] were also reported. Integration of Microstrip ring with various solid-state devices was realized to perform tuning, switching, amplification, oscillation, and optoelectronic functions. In the following sub-section, the EM coupling between microstrip ring resonators and their applications in filter design are discussed.

2.3.1. Ring Coupling Structures

As seen in Fig. 2.5, there are three basic coupling structures encountered in cross-coupled filters [16]. These different coupling structures arise from the different orientations of open-loop square resonators separated by a distance. Each of the open-loop resonators is essentially a folded half-wavelength resonator. It is known that the maximum electric coupling in a single resonator occurs at the side of the open-gap, whereas the maximum magnetic coupling occurs at the opposite side of the maximum electric field. This is because the electric/magnetic fringe fields are stronger at the sides where electric/magnetic field distributions are strong. Maximum electric coupling is obtained when the open-ends of the resonators are placed side by side as shown in Fig. 2.5(a). Similarly, maximum magnetic coupling is obtained if the unopened sides of the resonators are placed side by side as shown in Fig. 2.5(b). Finally, when the resonators

are placed as shown in Fig. 2.5(c), both strong magnetic and strong electric couplings are obtained, which is referred to as mixed coupling.

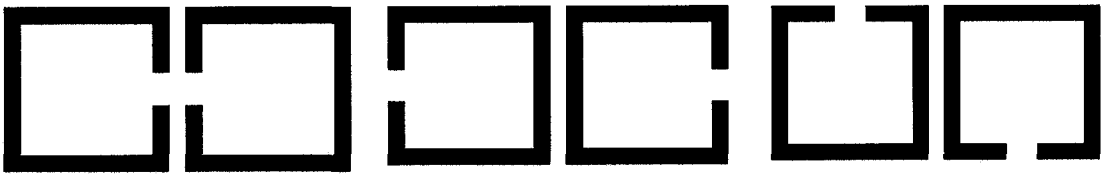

Fig. 2.5. Different coupling methods: (a) electric coupling, (b) magnetic coupling and (c) mixed coupling [16].

2.3.2. Coupling Models of Ring Structures

2.3.2.1. Electric Coupling

An equivalent lumped model for electric coupling resonators is shown in Fig. 2.6(b), where L and C correspond to self-impedance and self-capacitance, and C_m represents the mutual capacitance between resonators. $(LC)^{-1/2}$ equals to angular frequency of uncoupled resonators. If an electrical wall is inserted in the symmetrical plane of such circuit model, the resonant frequency of the resultant circuit is

$$f_e = \frac{1}{2\pi\sqrt{L(C+C_m)}}. \tag{2.8}$$

The resonant frequency is lower than of the uncoupled single resonator, which can physically be explained by the coupling effect which enhances the charge storing capacity of the resonator when the electrical wall is inserted. As expected, inserting a magnetic wall (open circuit) increases the resonant frequency which is given by

(a) (b)

Fig. 2.6. (a) Electric coupling structure and (b) its equivalent circuit.

$$f_m = \frac{1}{2\pi\sqrt{L(C - C_m)}}. \tag{2.9}$$

The equations (2.8) and (2.9) can be used to obtain the electric coupling coefficient

$$K_e = \frac{f_m^{\,2} - f_e^{\,2}}{f_m^{\,2} + f_e^{\,2}} = \frac{C_m}{C}. \tag{2.10}$$

It is also important to note that K_e is identical to the ratio of coupled electric energy to stored energy of the uncoupled single resonator.

2.3.2.2. Magnetic Coupling

An equivalent lumped model for magnetic coupling resonators is shown in Fig. 2.7(b), where L and C correspond to self-impedance and self-capacitance, and L_m represents the mutual inductance between resonators. In a similar manner, by inserting an electrical wall and a magnetic wall respectively, two corresponding resonant frequencies are given by

$$f_e = \frac{1}{2\pi\sqrt{C(L - L_m)}} \tag{2.11}$$

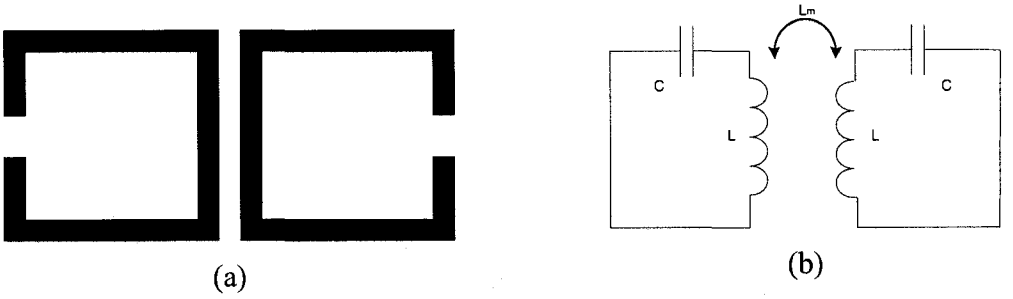

(a) (b)

Fig. 2.7. (a) Magnetic coupling structure and (b) its equivalent circuit.

and

$$f_m = \frac{1}{2\pi\sqrt{C(L+L_m)}}. \tag{2.12}$$

The equations (2.11) and (2.12) are used to obtain the magnetic coupling coefficient

$$K_m = \frac{f_e^{\,2} - f_m^{\,2}}{f_e^{\,2} + f_m^{\,2}} = \frac{L_m}{L}. \tag{2.13}$$

It is also important to mention that K_m is identical to the ratio of coupled magnetic energy to the stored energy of uncoupled single resonator. Most importantly, K_m and K_e are in reverse phases, which is the crucial property of the cross-coupled filters.

2.3.2.3. Mixed Coupling

In the mixed coupling structure, both magnetic and electric couplings are strong and comparable to each other so that neither of them could be ignored. The coupling structure of this situation is called mixed coupling. By inserting an electrical wall and a magnetic wall respectively, the resonant frequencies of mixed coupling resonators can be stated as

$$f_e = \frac{1}{2\pi\sqrt{(C - C_m)(L - L_m)}} \tag{2.14}$$

and

$$f_m = \frac{1}{2\pi\sqrt{(C + C_m)(L + L_m)}}. \tag{2.15}$$

Here, L and C correspond to self-impedance and self-capacitance. C_m and L_m represent the mutual capacitance and mutual inductance between resonators. Using (2.14) and (2.15), the mixed coupling coefficients become,

$$K_B = \frac{f_e^2 - f_m^2}{f_e^2 + f_m^2} = \frac{CL_m + LC_m}{LC + L_m C_m}. \tag{2.16}$$

It is reasonable to assume $L_m C_m << LC$ so that

$$K_B \approx \frac{L_m}{L} + \frac{C_m}{C} = k_m + k_e. \tag{2.17}$$

As seen, mixed coupling is the superposition of the electric and the magnetic coupling in phase, which is the result that had been expected.

2.3.3. Frequency Response and Quality Factor of Ring Resonators

If the resonator is symmetrical, it could form a two-port network, as shown in Fig. 2.8, where T - T' represents the symmetrical plane and the LC resonator has been separated into two symmetrical parts. When the T - T' is short-circuited, it may be noted that

$$Y_{ino} = \infty, \tag{2.18}$$

and

$$S_{11o} = \frac{G - Y_{ino}}{G + Y_{ino}} = -1, \tag{2.19}$$

where Y_{ino} and S_{11o} are the odd-mode input admittance and reflection coefficient at port 1, respectively. Alternatively, replacing the T - T' plane with an open circuit yields the corresponding parameters for the even mode:

$$Y_{ine} = j\omega_0 C\Delta\omega/\omega_0, \tag{2.20}$$

and

$$S_{11e} = \frac{G - Y_{ine}}{G + Y_{ine}} = \frac{1 - jQ_e\Delta\omega/\omega_0}{1 + jQ_e\Delta\omega/\omega_0}, \tag{2.21}$$

where $\omega_0 = 1/\sqrt{LC}$ and the approximation $(\omega^2 - \omega_0^2)/\omega \approx 2\Delta\omega$ with $\omega = \omega_0 + \Delta\omega$ has been made. Using (2.19) and (2.21), it can be noted that

$$S_{21} = \frac{1}{2}(S_{11e} - S_{11o}) = \frac{1}{1 + jQ_e\Delta\omega/\omega}, \tag{2.22}$$

whose magnitude is given by

$$|S_{21}| = \frac{1}{\sqrt{1 + (Q_e\Delta\omega/\omega_0)^2}}. \tag{2.23}$$

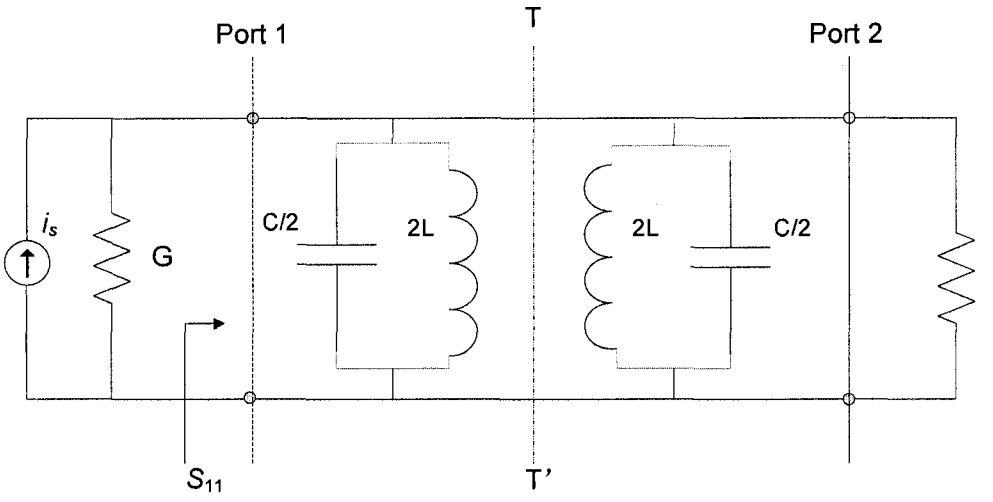

Fig. 2.8. Equivalent circuit of the resonator with double loading.

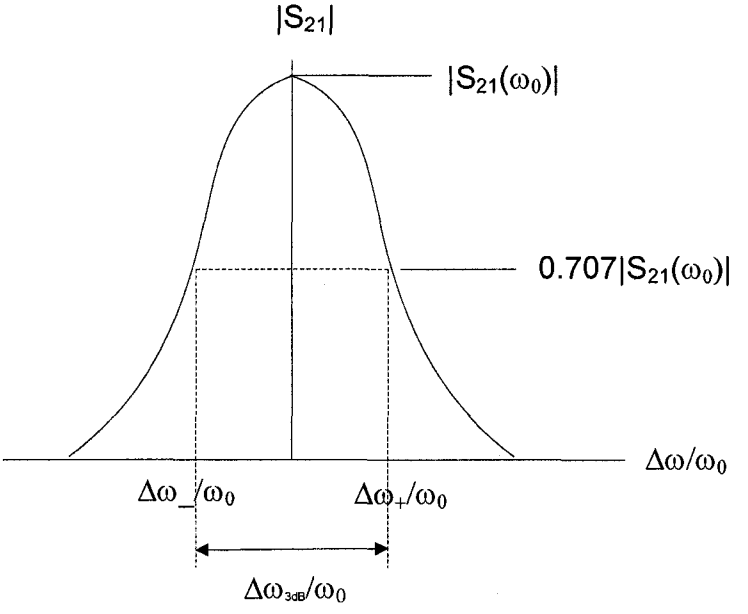

Fig. 2.9 Resonant amplitude response of S_{21} for the circuit in Fig. 2.8.

Shown in Fig. 2.9 is a plot of | S_{21} | against $\Delta\omega/\omega_0$. At resonance, $\Delta\omega = 0$ and | S_{21} | reaches its maximum value, namely | $S_{21}(\omega_0)$ | =1. When the frequency shifts such that

$$Q_e \frac{\Delta\omega_{\pm}}{\omega_0} = \pm 1, \tag{2.24}$$

the value of | S_{21} | has fallen to 0.707 (-3dB) of its maximum value according to (2.22). Based on (2.24), a bandwidth is defined as

$$\Delta\omega_{3dB} = \Delta\omega_{+} - \Delta\omega_{-} = \frac{\omega_0}{(Q_e/2)}, \tag{2.25}$$

where $\Delta\omega_{3dB}$ is the bandwidth for which the attenuation for S_{21} is up 3 dB from that at resonance, as indicated in Fig. 2.9. Define a doubly loaded external quality factor Q_e' as

$$Q_e' = \frac{Q_e}{2} = \frac{\omega_0}{\Delta\omega_{3dB}}. \tag{2.26}$$

Using (2.26) to extract the Q_e' first, then the singly loaded external quality factor Q_e is simply the twice of Q_e'.

It should be mentioned that even though the formulations made in this section are based on the parallel resonator, there is no loss of generality because the same formulas as (2.26) can be derived for the series resonator as well.

2.4. Ring Resonator Filter

As can be seen Fig. 2.10(a), a ring resonator filter [16] was implemented using two hairpin resonators with asymmetric feed lines. The dominant coupling of such filter structure is electrical coupling, whose performances have been introduced in previous subsections. The gaps between two hairpin resonators act as mutual capacitance, which can be adjusted to achieve optimal frequency responses, *i.e.* widest bandwidth and lowest loss. Fig. 2.11(b) shows the simulated *S*-parameters of traditional ring resonator filters with a gap of 0.06 mm. The ring resonator filter features a center frequency of 6.5 GHz, a bandwidth of 550 MHz, and a maximum return loss of 24 dB.

However, in a typical fabrication process employed for microstrip printed structure, the closest distance that can be manufactured is 0.13 mm. Such gap width can not provide satisfactory strong coupling between end-coupled resonators. As such, degradations in the filtering behavior in terms of high insertion loss and limited bandwidth are inevitable. In chapter 4, an improved ring structure is proposed to overcome the limitation posed by the fabrication process.

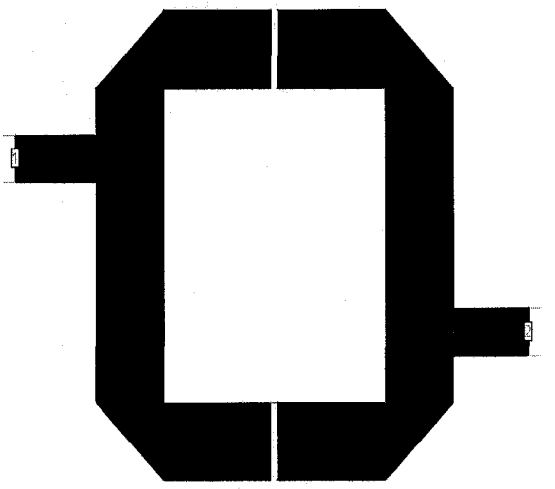

(a)

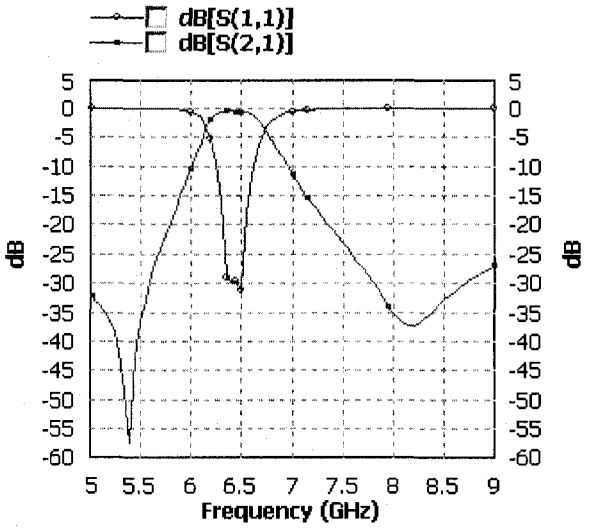

(b)

Fig. 2.10. (a) Layout of traditional ring resonator filters with a gap of 0.06 mm and (b) its simulation results.

Chapter 3

CAD of Composite Right/Left-Handed Bandpass Filters

The fundamental EM properties of LHMs and the physical realization of LHMs have been reviewed in chapter 2. The general TL approach provides insight into the physical phenomena of LHMs and provides an efficient design tool for LH applications. Based on the LH-TL units reported in [8], several microstrip bandpass filters have been designed with compact size, low loss or flat band, which enhance performances of MMIC system.

Currently, LHMs are considered to be a more general model of composite right/left-hand (CRLH) structures [26], which also include RH effects that occur naturally in practical LHMs. Metamaterials with RH and LH properties known as CRLH metamaterials have led to the development of several novel microwave devices.

In this chapter, a brief overview of CRLH-TL theory is presented. Based upon this theory, a new compact bandpass filter structure exploiting CRLH-TL concepts is

presented in section 3.1. Compared to traditional filter structures, the proposed filter is compact and provides relatively flat passband and wider bandwidth. Physical dimensions of the filter, *i.e.* design variables, can be adjusted to meet the given specifications. Based on the simulation results, a new CAD algorithm for fully-automated design of the filter is presented in section 3.2. The algorithm begins with the initialized values of physical dimensions. Enriched by the tuning knowledgebase compiled as part of the work, the physical dimensions are then adjusted iteratively. At the end of each iteration, the algorithm verifies if the specifications have been met, and continues or terminates accordingly. Section 3.3 presents concluding remarks. The related work has already been published in [42] and [43].

3.1 Proposed CRLH Bandpass Filter Structures

3.1.1 CRLH Theory

The homogeneous lossless models of a RH, LH, and CRLH-TL are illustrated in Fig. 3.1(a), (b), and (c), respectively. The RH-TL model and LH-TL model, which are dual of each other, have been discussed in Chapter 2. It is to be noted that in reality, a pure LH structure is not possible because of unavoidable RH parasitic series inductance and shunt capacitance effects (parasitic capacitance is due to development of voltage gradients, and unavoidable parasitic inductance is due to the current flow along the metallization). Therefore, a CRLH structure represents the most general form of a structure with LH attributes. The general CRLH-TL model shown in Fig. 3.1(c) consists of an inductance

L_R' in series with a capacitance C_L', and a shunt capacitance C_R' in parallel with an inductance L_L'.

The propagation constant of a TL is given by $\gamma = \alpha + j\beta = \sqrt{Z'Y'}$, where Z' and Y' are, the per-unit length impedance and per-unit length admittance respectively. In the case of the CRLH-TL shown in Fig. 3.1 (c)), Z' and Y' are defined as

$$Z'(\omega) = j(\omega L'_R - \frac{1}{\omega C'_L}), \tag{3.1}$$

$$Y'(\omega) = j(\omega C'_R - \frac{1}{\omega L'_L}). \tag{3.2}$$

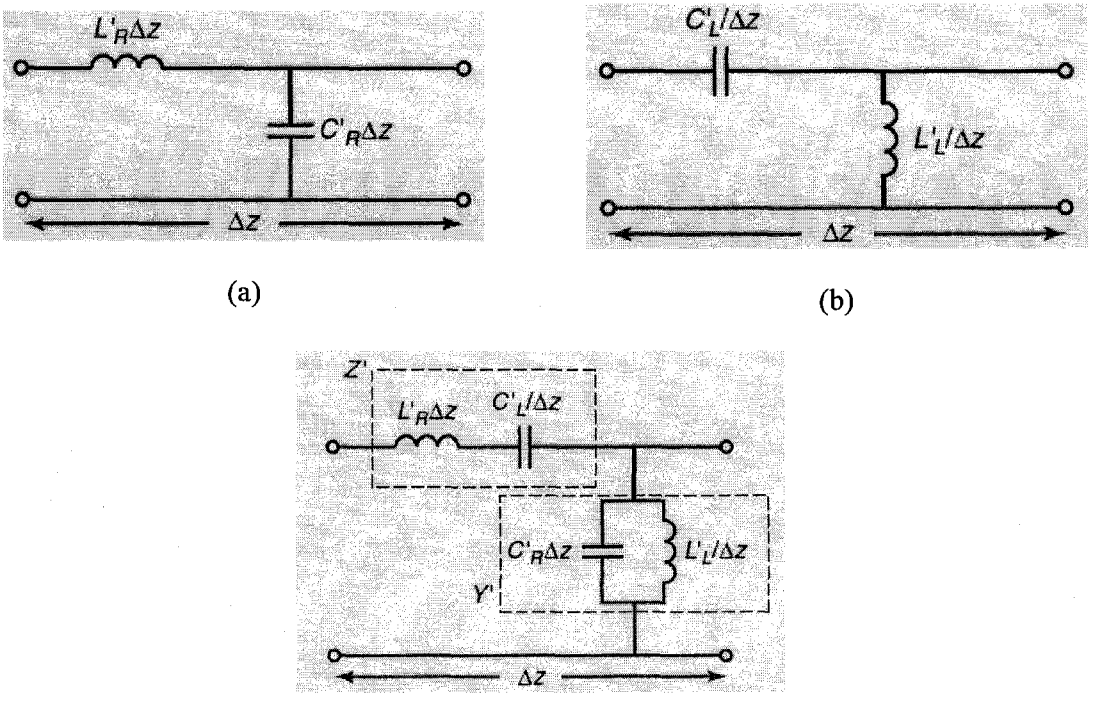

Fig. 3.1. Equivalent circuit model of lossless (a) RH-TL, (b) LH-TL, and (c) CRLH-TL

[26].

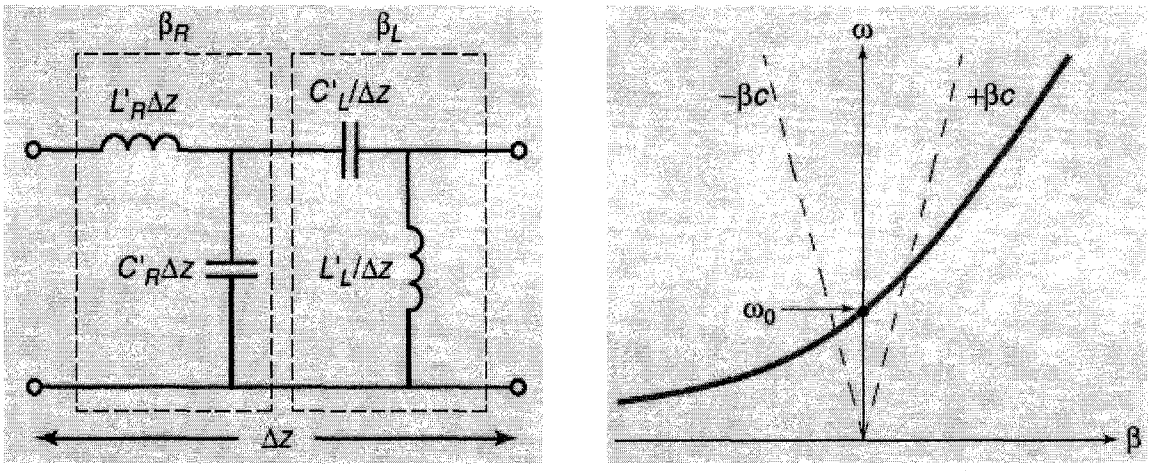

(a) (b)

Fig. 3.2. (a) Simplified equivalent circuit model and (b) dispersion diagram of CRLH-TL [26].

When the series and shunt resonances are equal,

$$L'_R C'_L = L'_L C'_R, \tag{3.3}$$

where LH and RH contribution exactly balance each other at a given frequency. This condition is called the balanced case, which results in the simplified circuit model as shown in Fig. 3.2(a). Under the condition of (3.3), the propagation constant can be expressed as

$$\beta = \beta_R + \beta_L = \omega\sqrt{L'_R C'_R} - \frac{1}{\omega\sqrt{L'_L C'_L}}, \tag{3.4}$$

where the phase constant distinctly splits up into the RH phase constant β_R and the LH phase constant β_L. As shown in Fig. 3.2(b), CRLH-TL is increasingly dispersive as

frequency increases, since the phase velocity ($v_p = \omega/\beta$) becomes increasingly dependent on frequency. CRLH-TL illustrates a dual nature, *i.e.* dominantly LH at low frequencies and dominantly RH at high frequencies. The balanced CRLH-TL's dispersion diagram of Fig. 3.2(b) indicates that the transition from LH to RH occurs at

$$\omega_0 = \frac{1}{\sqrt[4]{L'_R C'_R L'_L C'_L}} = \frac{1}{\sqrt{L'C'}}, \tag{3.5}$$

where ω_0 is referred to as the transition frequency [26]. As can be seen in Fig. 3.2(b), there is a seamless transition from LH to RH for the balanced case. As a result, the balanced CRLH-TL's dispersion curve does not have a stop-band. It is to be noted that although β is zero at ω_0, which corresponds to an infinite guided wavelength ($\lambda_g = 2\pi/|\beta|$), wave propagation still occurs since v_g is nonzero at ω_0. In addition, at ω_0, the phase shift for a TL of length d is zero ($\varphi = -\beta d = 0$). Phase advance ($\varphi > 0$) occurs in the LH frequency range ($\omega < \omega_0$), and phase delay ($\varphi < 0$) occurs in the RH frequency range ($\omega > \omega_0$).

The unique feature of CRLH metamaterials is that $\beta = 0$ can be achieved at a nonzero frequency ω_0. When $\beta = 0$, there is no phase shift across transmission medium since the phase shift φ is determined by $\varphi = -\beta d = 0$. In addition, it can be shown that the resonance is independent of the length of the structure but is only dependent on the reactive loadings. Such particular property of CRLH-TL can be utilized to design a bandpass filter which resonates at ω_0. Since the resonance is independent of physical dimensions, microwave filters using CRLH-TL structures have a potential for effective volume minimization.

3.1.2 Microstrip CRLH Bandpass Filter

Two inter-digital capacitors in series are considered as a LH-TL unit. The outer arms of these capacitors whose edges are grounded by vias act as shunt inductors. EM simulations performed using Zeland's *IE3D* and presented in Fig. 3.3 (b) show a highpass behavior. As discussed in the previous subsection, any LH-TL is a CRLH-TL because of unavoidable parasitic series inductance and shunt capacitance resulting in a RH contribution that increases with the frequency. Thus, a CRLH-TL can be considered to be composed of LH featuring lowpass characteristics at lower frequencies and RH featuring highpass characteristics at higher frequencies. As such, the CRLH-TL structure can potentially realize bandpass characteristics.

Motivated by the above idea, one interdigital capacitor of Fig. 3.3 (a) is selected to implement a CRLH bandpass filter. By adjusting its physical dimensions, *i.e.* length (*D*) of outer arms, length (*T*), width (*M*), number of fingers (*N*) and gap between fingers (*S*), the structure can be made to provide bandpass characteristics shown in Fig. 3.4. The substrate height is 0.254 mm and ε_r is 2.2. Using Zeland's *IE3D*, the EM simulation results of Fig. 3.4(a), illustrated in Fig. 3.4(b), exhibit a center frequency f_0 = 8.4 GHz, a 3 dB fractional bandwidth = 49.4%, an insertion loss of 0.33 dB at 8.3 GHz, and a return loss > 15 dB in the 6.8-9.5 GHz range. The low losses and extremely wide bandwidth of the proposed structure make it attractive for wideband communication applications. Fig. 2.4(c) shows the RH and LH regions of the new filter by means of the positive or negative value of β, which confirms that the structure is indeed a CRLH-TL, and also indicates the passband of the bandpass filter.

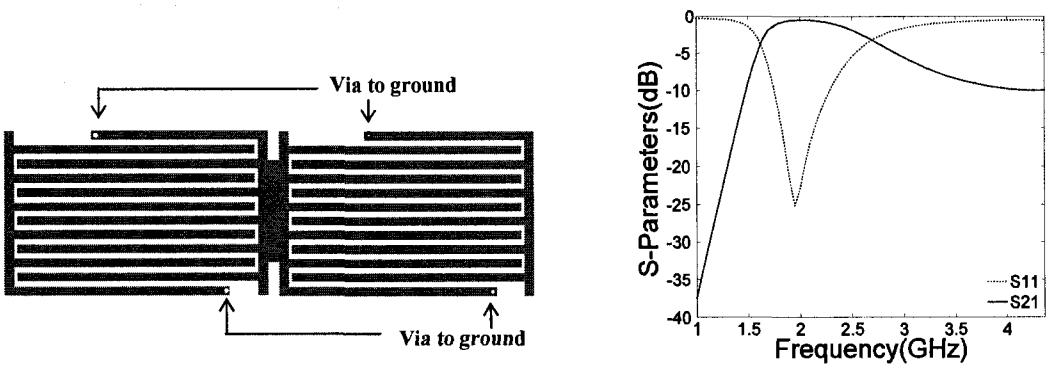

(a) (b)

Fig. 3.3. (a) Layout of a single unit of the LH-TL and (b) its simulated *S*-parameters.

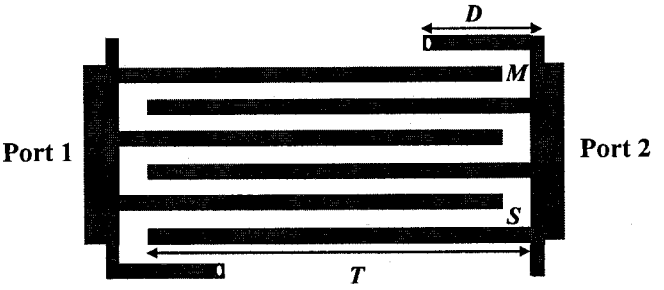

(a)

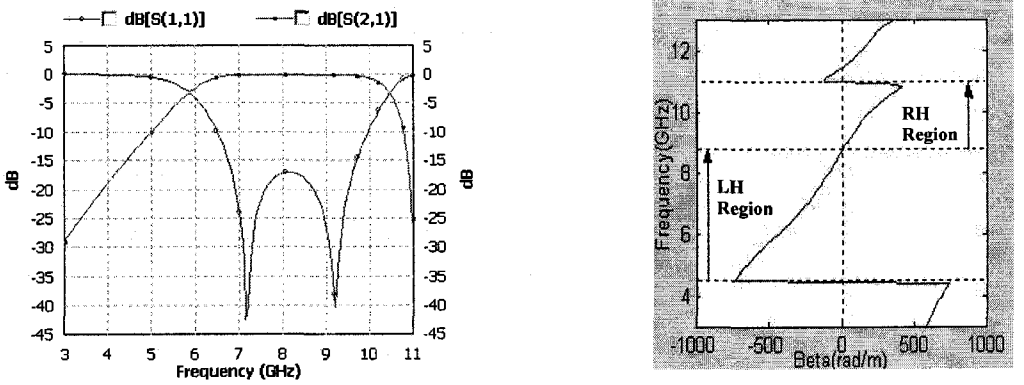

(b) (c)

Fig. 3.4. (a) Layout of the CRLH-TL filter with $D = 1.1$mm, $T = 3.925$mm, $M = 0.1$mm, $N = 6$ and $S = 0.1$mm, (b) simulated *S*-parameters of the CRLH filter, and (c) ω-β diagram resulting from $\varphi(S_{21})$.

3.1.3 Volume Comparison

The resonance of the CRLH filter is independent of its physical dimensions. Hence, microwave components implemented by means of CRLH-TL structures may lead to effective size minimization. In this subsection, the proposed CRLH bandpass filter is compared with existing traditional filter structures.

In Fig. 3.5, two traditional microstrip filter structures, *i.e.* the microstrip parallel coupled bandpass filter (see Fig. 3.5(a)) and microstrip hairpin bandpass filter (see Fig. 3.6(a)) are compared with the proposed CRLH bandpass filter. All three structures exhibit comparable bandpass performances (see Fig. 3.5(b) and Fig. 3.6(b)), *i.e.*, center frequency f_0 = 8.3 GHz, 3-dB fractional bandwidth ≈ 50% and maximum passband attenuation = 0.3 dB. The dimensions of these structures are shown in Table 3.1. As can be inferred from Table 3.1, the proposed simple yet interesting structure leads to considerable real-estate savings as compared to traditional microstrip hairpin filter and parallel coupled-line filter.

Table 3.1

Size comparison between proposed filter and traditional filters

Filter Style	Size
Proposed CRLH Bandpass Filter	4.23×1.5 mm^2
Traditional Coupled Microstrip RH-TL Filter	28.5×1.1 mm^2
Traditional Microstrip Hairpin Filter	7.8×9.8 mm^2

(a)

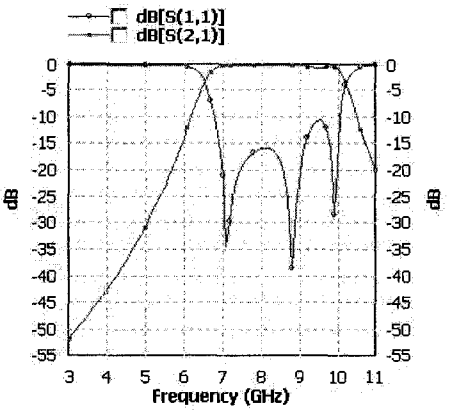

(b)

Fig. 3.5(a) Layout of the microstrip parallel coupled bandpass filter and (b) its simulated *S*-parameters.

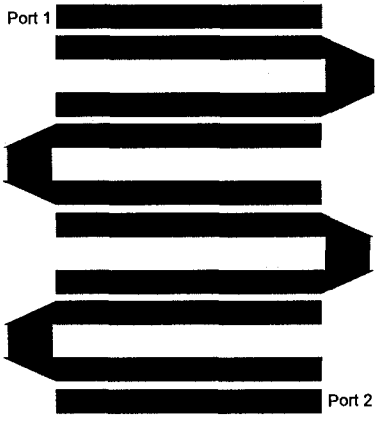

(c)

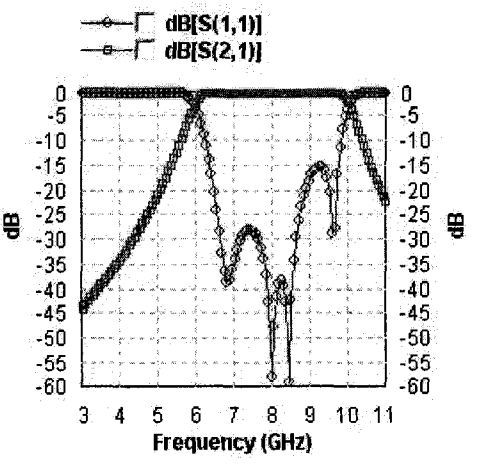

(d)

Fig. 3.6(a) Layout of the microstrip hairpin bandpass filter and (b) its simulated *S*-parameters.

3.2 CAD Algorithm for the CRLH Filter

Design/tuning of RF/microwave circuits is multi-dimensional and therefore complex. Several strategies have been employed in the CAD area to address this challenge [18]. Current CAD tools offer various benefits such as lower product development costs and greatly shortened design cycles. CRLH-TL structure has unique value for realizing bandpass filters with relatively smaller volumes. Since CRLH filter is a new concept, developing a CAD method for such filters is of potential interest to designers.

3.2.1 Analysis of Simulation Results

As a first step toward developing a fully-automated CAD tool for the design of proposed CRLH filters, a simulation study has been carried out. The design parameters D, T, M and N (see Fig. 3.4(a)) have been varied (or swept) and their effect on various design specifications has been examined. Some of the results of the study are shown in Fig. 3.7. In Fig. 3.7, each design parameter is varied, while keeping the other parameter values constant. Consequently, the overall effect of each design parameter on the filter's specifications is clearly brought out:

- The length D of the arm-inductors has great effect on the impedance matching of the filter, whereas it has minimal influence on the central frequency and passband.
- The length T of the inter-digital capacitor influences the central frequency slightly. More specifically, central frequency decreases with increasing T.

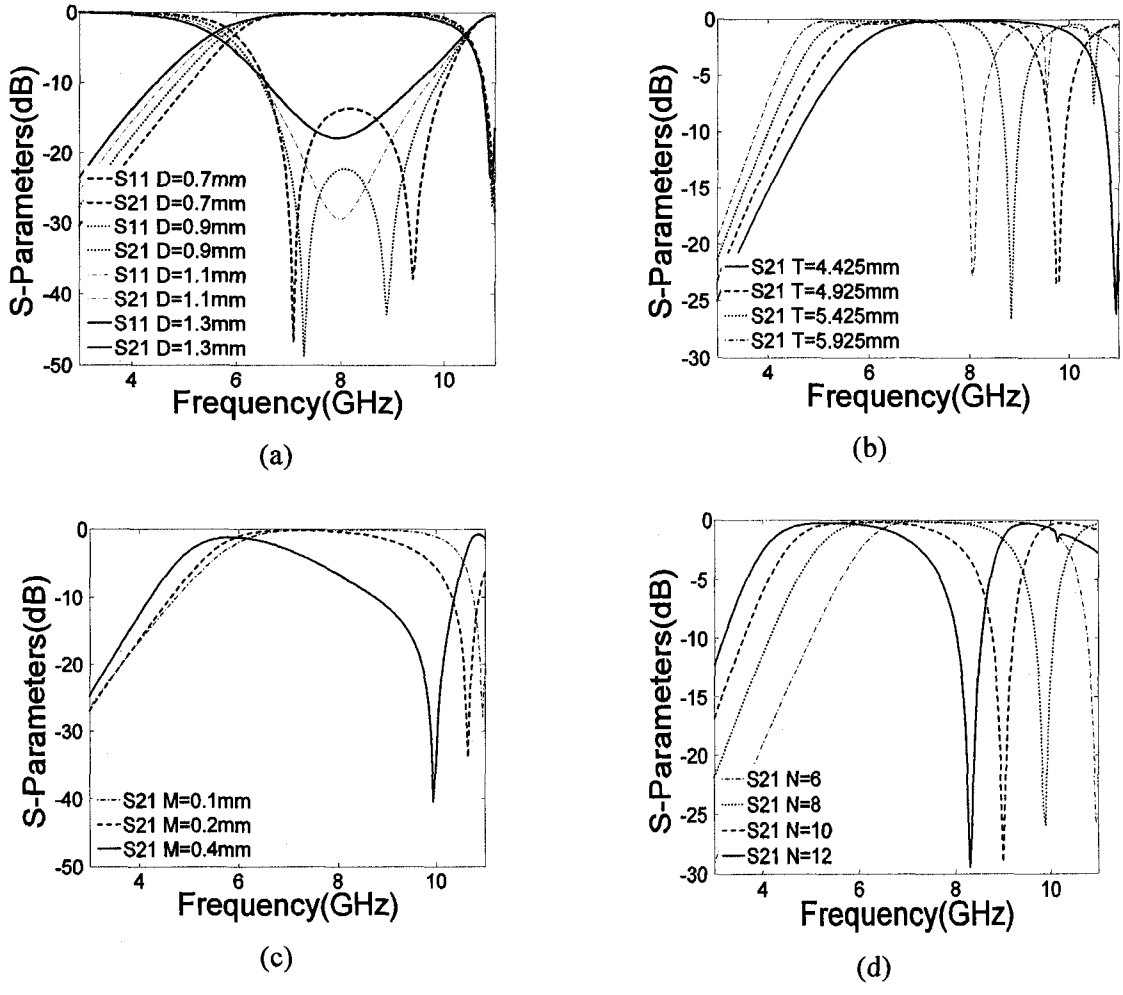

Fig. 3.7. Simulated *S*-parameters of Fig. 3.4 (a) with different values of (a) *D*, (b) *T*, (c) *M* and (d) *N*.

- The width *M* of the fingers influences central frequency and bandwidth simultaneously. Increase of *M* results in decrease of the central frequency and bandwidth.
- The number of fingers *N* has considerable influence on the central frequency. More specifically, central frequency decreases sharply when *N* increases.

The sensitivity information has been analyzed and compiled into a knowledge base shown in Table 3.2. Such knowledge base identifies the design parameter(s), which highly influence each of the filter's specifications. For instance, increasing *T* results in a slightly negative shift in centre frequency, while decreasing *M* results in a positive shift in both centre frequency and upper edge frequency. *NC* stands for "negligible change".

Table 3.2
Knowledge Base for the CAD Methodology

Tuning Action	**Centre Frequency**	**3dB Bandwidth**	**Edge Frequencies**	
			Lower	**Upper**
Change *D* ↑/↓	NC	NC	NC	NC
Change *T* ↑/↓	↓/↑ (slight change)	NC	↓/↑	↓/↑
Change *M* ↑/↓	↓/↑	↓/↑	NC	↓/↑
Change *N* ↑/↓	↓/↑ (sharp change)	NC	↓/↑	↓/↑
Note: Maximum pass-band attenuation and minimum stop-band attenuation are observed when "impedance matching" is satisfied.				

3.2.2 Design Algorithm

Based on the knowledge base in Table 3.2, a CAD algorithm has been developed for automated design of CRLH filers (see Fig. 3.8). The automated design procedure begins with the users' specifications which includes the center frequency, bandwidth, passband/stopband attenuation, etc. The specifications are first analyzed by the computer, and an initial set of numerical values of physical parameters are produced to implement the initial layout of a CRLH filter.

After simulating the initial filter structure, the bandwidth specification is checked first, since only M among the four parameters influences bandwidth considerablely. Once the required bandwidth is achieved by tuning M, the algorithm then checks the central frequency specification. As can be seen in Fig. 3.8, coarse adjustments by tuning N and fine adjustments by tuning T are operated sequentially/iteratively, to achieve the required central frequency. The final step is to adjust D to obtain the best matching, since D minimally affects the bandwidth and center frequency, but is sensitive to impedance matching. In the end, the CAD algorithm obtains the final values of geometrical parameters of the CRLH filter.

A counter that records the loop time is added in the algorithm. In case the automated design algorithm exceeds the maximum allowed simulation times; the simulation will be terminated by the counter. In the next subsection, a step by step example will be shown to demonstrate the effectiveness of the proposed CAD method for CRLH filters.

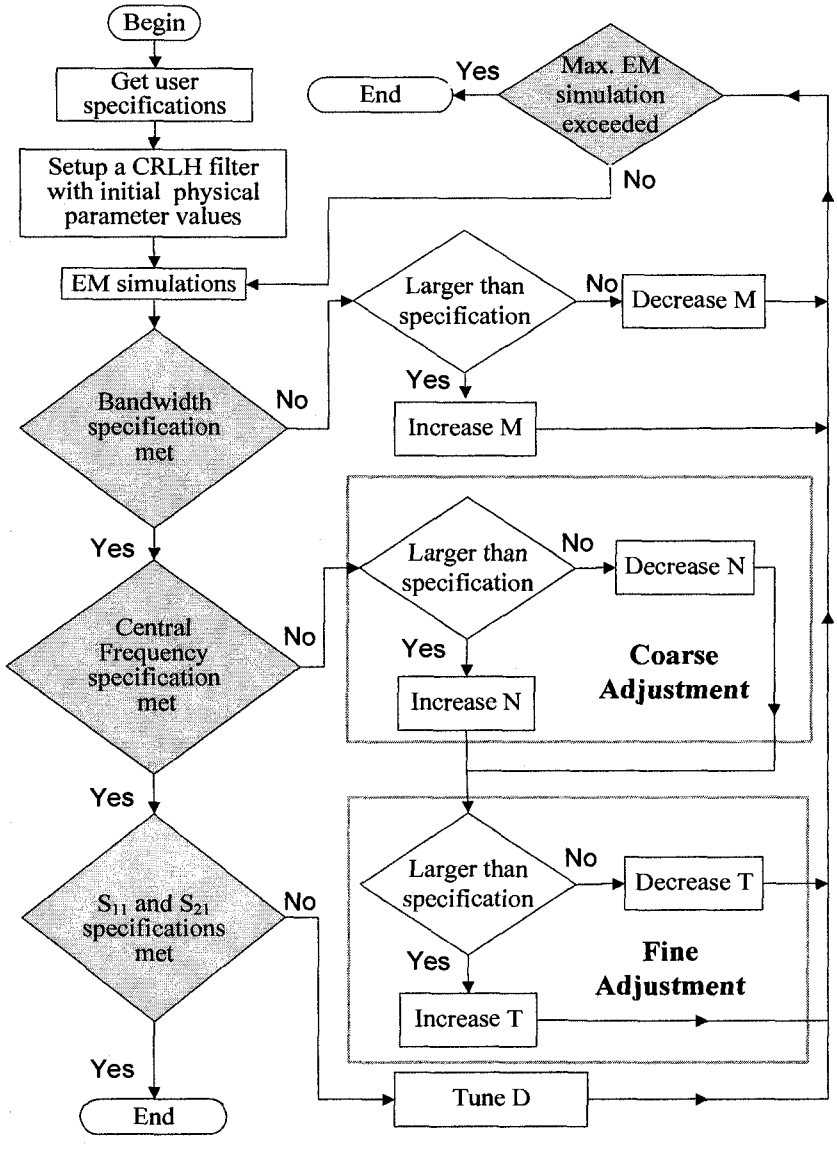

Fig. 3.8. Flow-chart of the routine that forms a basis for the proposed CAD methodology.

3.2.3 Design Example

In this subsection, an example of CRLH filter design using the proposed CAD methodology is presented. User-specifications include maximum passband attenuation = 0.1 dB, minimum stopband attenuation = 25 dB, central frequency = 6 GHz and 3dB bandwidth = 2.5 GHz. Initial values of physical parameters are considered as D=2mm, T=4mm, M=0.8mm, and N=6.

Step 1: An initial *IE3D* simulation is performed with some initial design parameter values. As may be seen in Fig. 3.9(a), the centre frequency is near 4 GHz and the width of the passband is almost zero.

Step 2: Based on the flow-chart, bandwidth specification is initially checked. The width of the passband can be increased by decreasing M, and this is a relatively simpler 1-dimensional design problem. Gradually decreasing M from 0.8 mm to 0.27 mm has resulted in a BW, which is closer to the given specification (see Fig. 3.9(b)). However, after this step, the centre frequency has shifted to around 7.5 GHz.

Step 3: The centre frequency (currently 7.5 GHz) can be "improved", *i.e.* decreased, by increasing N. Changing N from 6 to 8 has resulted in f_0 = 6.25 GHz, which is closer to the given specification (see Fig. 3.9(c)). This change is categorized as a coarse adjustment. The influence to the bandwidth by this change can be ignored.

Step 4: A fine adjustment is performed by increasing T from 4mm to 4.16mm such that the specification f_c = 6GHz has been met precisely (see Fig. 3.9(d)). This change is categorized as a fine adjustment. The influence on the bandwidth by the change can also be ignored.

Step 5: After meeting the specifications of centre frequency and bandwidth, the matching is considered as the last step. In order to meet the desired values of attenuation, *i.e.* S_{11} and S_{21}, D has been adjusted from 2mm to 0.49mm for impedance matching. As seen in Fig. 3.9. (e), all required specifications have been met. The final values of geometrical parameters are $D = 0.49$mm, $T = 4.16$mm, $M = 0.27$mm and $N = 8$.

3.3 Summary

Owing to the negative and nonlinear nature of phase constant (β) versus frequency, CRLH-TL can have resonance which is independent of physical dimensions. As such, CRLH structures seem promising in terms of size minimization of microwave circuits. In this chapter, a new microstrip CRLH-TL bandpass filter has been proposed. The simulation results of CRLH filter has shown a minimum insertion loss of 0.33 dB and a wide 3-dB fractional bandwidth of 49.4%. Moreover, its volume (4.23×1.5 mm^2) is about 10 times smaller than traditional printed filters with comparable frequency response. In addition, a geometrical parameter analysis of the CRLH filter has been carried out. This analysis has lead to the development of an automated design algorithm for CRLH filters. The proposed algorithm has been validated through a practical example.

Since the unique β of CRLH metamaterials has more connection to phase responses, CRLH metamaterials are potentially providing more applications having specific phase specifications, such as CRLH antenna, CRLH directional coupler and so on.

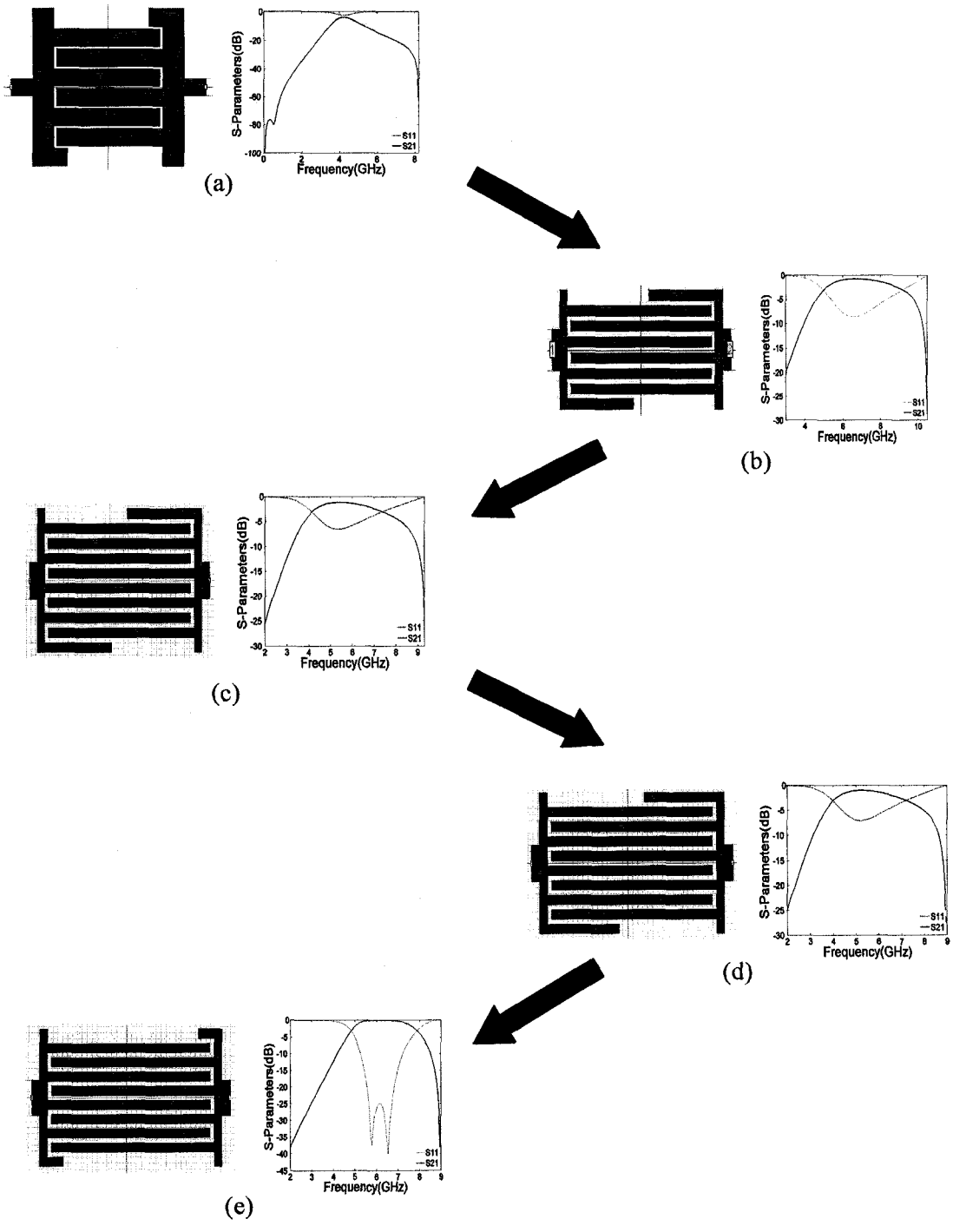

Fig. 3.9 Automated CRLH filter design (a) step 1 with D=2mm, T=4mm, M=0.8mm, N=6, (b) step 2 with D=2mm, T=4mm, M=0.27mm, N=6, (c) step 3 with D=2mm, T=4mm, M=0.27mm, N=8, (d) step 4 with D=2mm, T=4.16mm, M=0.27mm, N=8, and (e) step 5 with D=0.49mm, T=4.16mm, M=0.27mm, N=8.

Chapter 4

Interdigital Ring Filters with Adjustable Bandwidth and Predictable Transmission Zeros

In the past three decades or so, ring resonators have been widely used in filters, oscillators, mixers, couplers, power dividers/combiners, antennas, frequency selective surfaces, and so forth. As mentioned earlier, the microstrip ring resonator was first proposed by P. Troughton in 1969 for the measurements of the phase velocity and dispersive characteristics of a microstrip line. In the following years, most applications were focused on the measurements of characteristics of discontinuities of microstrip lines. In the 1980s, applications using ring circuits as antennas, filters, mixers, baluns, and couplers were reported. The ring resonator only support waves whose guided wavelengths equal to an integral multiple of the ring circumference. Using this ring circuit, many more circuits can be created by cutting a slot, adding a notch, cascading two

or more rings, implementing some solid-state devices, and so on.

It has been reported recently that hairpin resonators with asymmetric input/output feed lines tapping on the first and the last resonators can be employed in the design of microstrip bandpass filters [27][28]. In contrast to traditional cross-coupled filters, hairpin-resonator filters offer lower insertion loss, sharper cutoff frequency response, and two transmission zeros lying on either sides of the passband. In the design of hairpin-resonator filters, a wider bandwidth can be achieved by improving the electromagnetic (EM) coupling between resonators, which can be realized by reducing gap and/or strip widths of resonators. However, such an approach can lead to a degradation in the filtering behavior in terms of low quality factor Q and high insertion loss. Moreover, the approach may require a high precision fabrication process for accurate gap/strip dimensions.

This chapter describes a practical limitation in designing traditional ring resonators. In order to overcome this challenge, a J-inverter topology [29]-[31] is explored to estimate EM coupling strengths of three different coupling structures. Based on the study, a new bandpass filter structure, which uses interdigital capacitors between hairpin resonators, is proposed. Such an arrangement helps to obtain a relatively stronger EM coupling and hence a relatively wider bandwidth as compared to edge-coupled hairpin filters. Two additional slots etched in the ground plane can help further enhance the bandwidth. The proposed structure exhibits two transmission zeros, one on each side of the passband. In order to estimate the positions of these transmission zeros, semi-analytical formulae are derived. The proposed filter allows certain flexibility in the design, *i.e.* ability to adjust the bandwidth by altering the geometrical parameters of the interdigital capacitors and/or

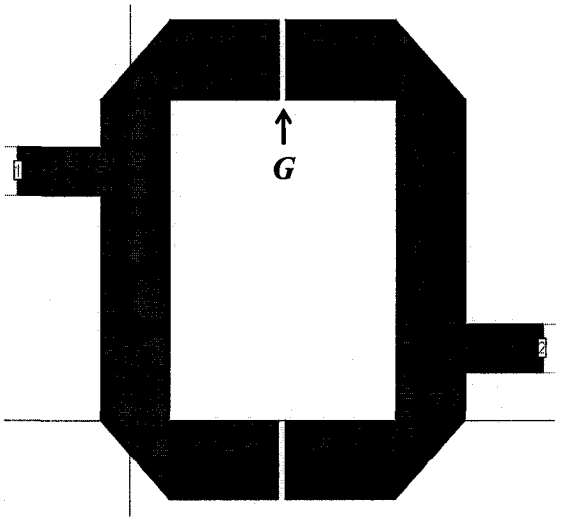

Fig. 4.1. Layout of a traditional edge-coupled bandpass filter.

the etched slots. Based on the proposed structures, cascaded bandpass filters are designed, fabricated and tested. The related work has been published in [44], and submitted in [45].

4.1 Limitation of Traditional Ring Resonator Filter

As can be seen in Fig. 4.1, a traditional ring resonator filter is implemented using two hairpin resonators with asymmetric feed lines. The gap G between two hairpin resonators acts as mutual capacitance, which can be adjusted to achieve optimal frequency response, *i.e.* wide bandwidth and low loss.

Fig. 4.2 (a)-(c) show the simulated S-parameters of traditional ring resonator filters with different G. As can be summarized from the three figures, with the decrease of distance between hair resonators from 0.08 mm to 0.04 mm, the filter shows wider bandwidth and better frequency responses. When G = 0.04 mm (see Fig. 4.2(c)), the filter

features a 3dB bandwidth of 650 MHz and a maximum return loss of 24.8 dB. However, in a typical fabrication process employed for microstrip structures, the closest distance that can be manufactured is 0.13 mm. As can be seen in Fig. 4.2 (d), with $G = 0.13$ mm, the 3dB bandwidth is 320 MHz and the maximum return loss is only 11.2 dB, both of which are not acceptable with respect to the given specifications of the filter.

In conclusion, traditional ring filters use open-end gaps to realize coupling, which may not be able to achieve strong enough coupling to achieve optimal responses. In order to overcome the drawback, the coupling strength of different microstrip structures is discussed in the next subsection and some additional structures are considered in ring resonators to attain strong coupling.

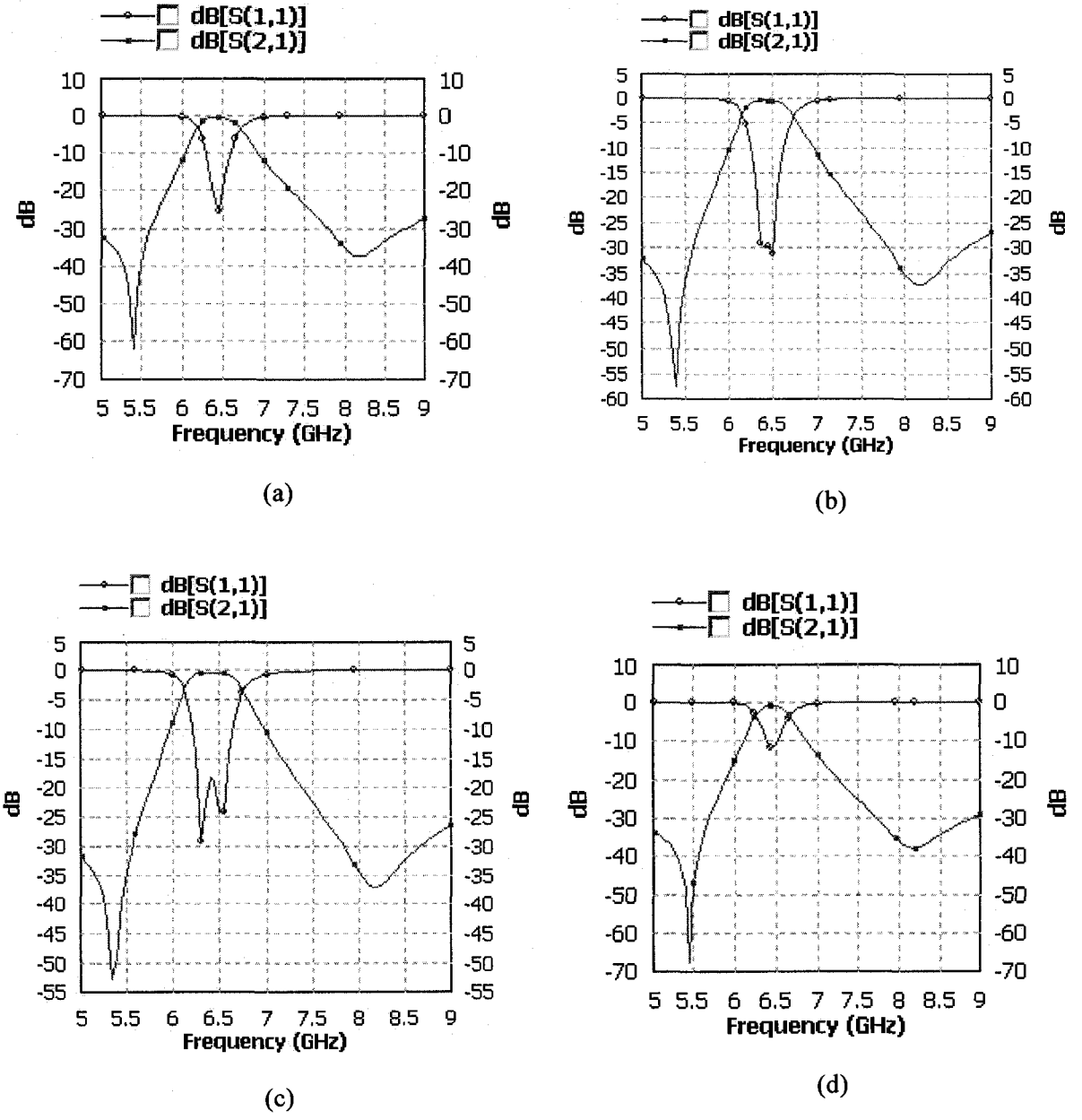

Fig. 4.2 Simulated *S*-parameters of the traditional ring resonator filters with G = (a) 0.08 mm, (b) 0.06 mm, (c) 0.04 mm, and (d) 0.13 mm.

4.2 Estimation of EM Coupling

Three different microstrip coupling structures, illustrated in Fig. 4.3, are considered. Fig. 4.3(a) shows an unbound end-to-end coupling gap with open-ends R_1 and R_2, and Fig. 4.3(b) shows a nine-finger interdigital capacitor. The structure in Fig. 4.3(c) is identical to that in Fig. 4.3(b) except that it has a rectangular ground-plane aperture below the interdigital capacitor. All three kinds of coupling structures have the same length. To investigate their coupling behaviors, these microstrip structures are initially modeled by using a 3D admittance–type MoM algorithm [31].

In the MoM algorithm, a pair of impressed electrical fields (E_1 and E_2) is introduced to formulate a deterministic MoM at two ports (P_1 and P_2) far away from the reference planes (R_1 and R_2). To accurately de-embed circuit parameters of these microstrip structures from the MoM calculation, the short-open calibration procedure [30] is deployed to remove error terms involved in the algorithm that allows extracting an equivalent circuit model at the reference planes (R_1 and R_2). In Fig. 4.3(d), an equivalent *J*-inverter network model for the coupling structures is presented, where the entire two-port coupled microstrip lines can be characterized by a *J*-inverter network model and two identical error terms [30]. The physical structure is modeled as an equivalent *J*-inverter network combined with two identical error terms [X_f]. The error terms relate to the approximation of source excitation and inconsistency between 2D and 3D MoM-based impedance definitions. They can effectively be evaluated and removed with the assistance of two numerical calibration standards, namely, short and open elements. As such, the circuit network of the microstrip structures in Fig. 4.3(a) ~ (c) can be explicitly

extracted as a general-purpose two-port admittance matrix that accounts for all of its discontinuity effects. Specifically, the *J*-inverter network consists of susceptance (*J*) and two equivalent electrical line lengths ($\theta/2$ each). For a symmetrical two-port *J*-inverter network [31], it can be noted that

$$\frac{J}{Y_0} = \frac{\tan(\theta/2) + \overline{B}_{11}}{\overline{B}_{12}\tan(\theta/2)} \tag{4.1}$$

and

$$\theta = -\tan^{-1}\left(\frac{2\overline{B}_{11}}{1-\overline{B}_{11}^{\,2}+\overline{B}_{12}^{\,2}}\right), \tag{4.2}$$

where Y_0 is the characteristic admittance of each line, B_{ij} is the susceptance of the corresponding *Y*-parameter from EM simulation, and $\overline{B}_{ij} = B_{ij}/Y_0$. Equations (4.1) and (4.2) allow the transformation from an admittance π-network to a *J*-inverter topology [31]. Fig. 4.4 shows normalized values of *J* for different coupling structures in the 1~8GHz frequency range. It can be seen that the parameter *J* varies nonlinearly with frequency *f*, exhibiting the frequency dispersion behavior. In addition, *J* increases noticeably from the structure of Fig. 4.3(a) to the structures of Figs. 4.3(b) and (c), with the structure of Fig. 4.3(c) exhibiting largest *J*. Since *J* is directly proportional to coupling strength [28], it can be inferred that coupling strength can be effectively enhanced by means of using interdigital capacitors and/or etched slots. In the following sections, a new class of miniaturised and broadband microstrip bandpass filters are investigated.

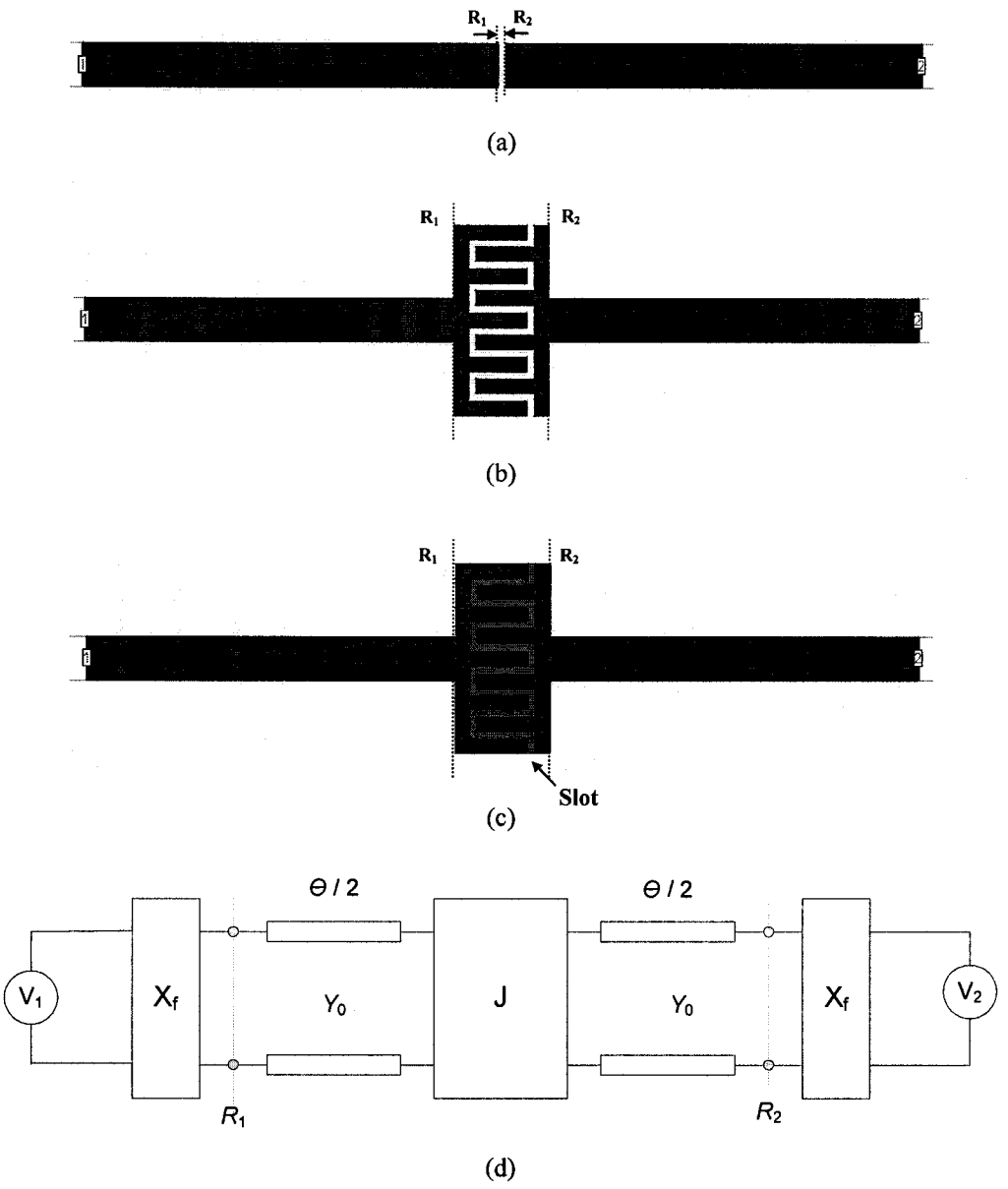

Fig. 4.3. (a) End-to-end coupled line, (b) Interdigital capacitor coupled line, (c) Interdigital capacitor coupled line with etched slot, and (d) Generalized *J*-inverter network model for the coupling structures.

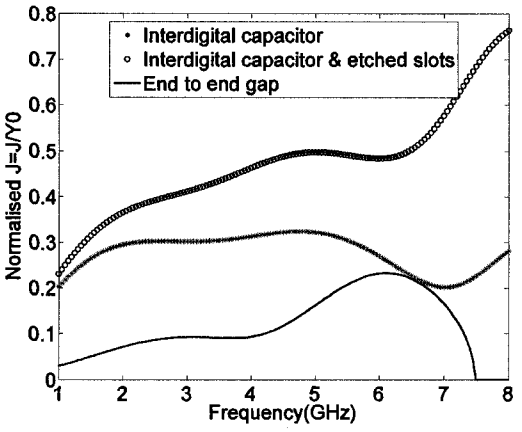

Fig. 4.4. Normalized susceptance (J/Y_0) for the coupling structures of Fig. 4.3.

4.3 Proposed Bandpass Filter Structures

A larger J implies a stronger coupling or smaller external quality-factor (Q_E) of a resonator [16]. The 3dB bandwidth of a filter can be expressed as

$$\Delta f_{3\text{dB}} = \frac{f_0}{(Q_{\text{E}}/2)}, \tag{4.3}$$

where f_0 denotes centre frequency. A larger J results in a smaller Q_{E} and hence a wider bandwidth. Therefore, different bandwidths can be achieved by choosing coupling structures with different J. Motivated by this, new bandpass filters are proposed based on the coupling structures noted in chapter 4.2. Fig. 4.5 shows the layout of the proposed bandpass filter and an illustrative comparison with a traditional edge-coupled filter [27][28]. The substrate thickness is 0.635 mm and dielectric constant (ε_r) is 10.2. As can be seen in Fig. 4.5(b), interdigital capacitors are introduced to substitute for the traditional gaps (see Fig. 4.5(a)) between microstrip hairpin resonators.

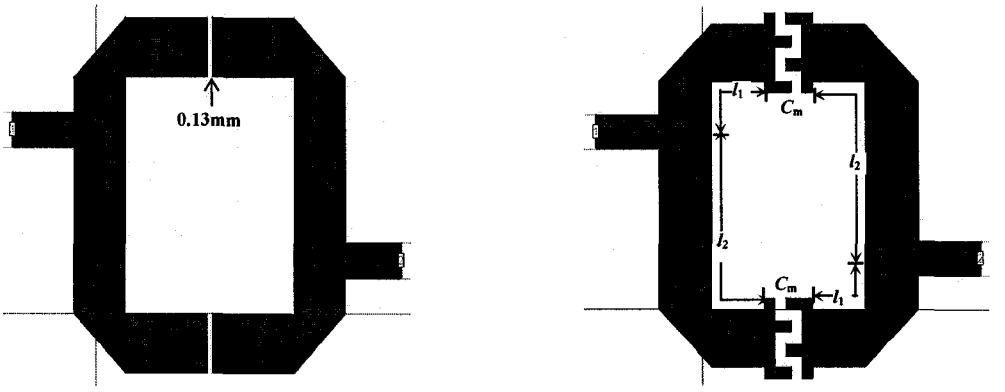

(a) (b)

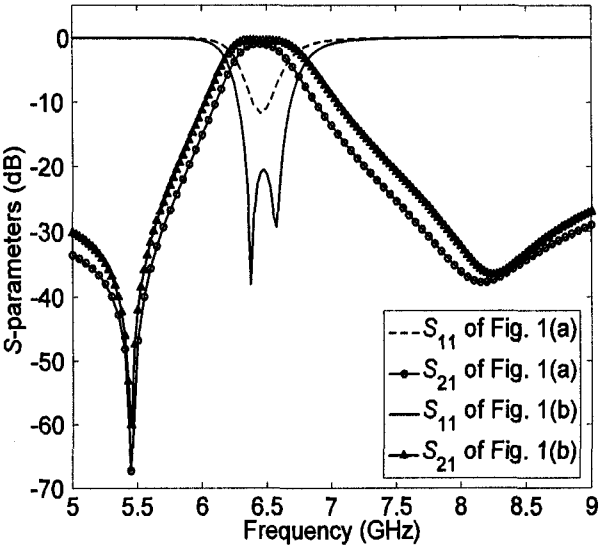

(c)

Fig. 4.5. (a) Layout of a traditional edge-coupled bandpass filter, (b) Layout of the proposed bandpass filter and (c) Comparison of simulated *S*-parameters of the proposed filter and the traditional filter.

In Fig. 4.5 (a), the width of the microstrip hairpin is 1 mm, and the gap is set to 0.13 mm (5 mil), which is the closest/smallest distance allowed by the fabrication process employed. Using Zeland *IE3D*, the EM simulation results of Fig. 4.5(a), illustrated in Fig. 4.5(c), exhibit an f_0 = 6.5 GHz, a 3 dB bandwidth = 375 MHz, an insertion loss of 0.83 dB at 6.49 GHz, a maximum return loss of 11 dB at 6.5 GHz, and two transmission zeros, one at 5.45 GHz with -66.34 dB rejection and the other at 8.3 GHz with -36.6 dB rejection. The relatively high loss and narrow bandwidth could not be improved due to gap limitation imposed by the fabrication process.

As shown in Fig. 4.5(b), the proposed structure uses two interdigital capacitors, each with 4 fingers, between the hairpin resonators. The length and width of the fingers are 0.3 mm and 0.2 mm respectively, and the gap between adjacent fingers is 0.2 mm. The EM simulation results of Fig. 4.5(b) are also illustrated in Fig. 4.5(c). Owing to a stronger coupling effect, the proposed filter exhibits a wider 3 dB bandwidth than traditional filter (602 MHz *vs.* 375 MHz), while its f_0 and locations of transmission zeros remain unchanged. Further, the proposed filter provides an insertion loss of 0.41 dB at 6.49 GHz and a return loss > 20 dB in the 6.34-6.61 GHz range, both of which are lower than those of the traditional hairpin filter. In conclusion, the increased mutual capacitance provided by interdigital capacitors helps to obtain a relatively stronger EM coupling and hence a relatively wider bandwidth compared to edge-coupled hairpin filters.

In both proposed and traditional structures, the dominant coupling is "electrical coupling" [16], which is due to the strong electric fringe fields near the open ends of the folded line. As such, the capacitance between two branches becomes an important

parameter to be examined. For both proposed and the traditional structures of Fig. 4.5, the mutual electrical coupling can be represented by a coefficient K_E, identical to the ratio of the coupled electric energy to the stored electric energy of an uncoupled single resonator *i.e.*

$$K_E = \frac{f_{r2}^{\,2} - f_{r1}^{\,2}}{f_{r2}^{\,2} + f_{r1}^{\,2}} = \frac{C_m}{C}. \tag{4.4}$$

In (4.4), C represents self-capacitance, C_m represents mutual capacitance, and f_{r1} and f_{r2} represent the lower and higher resonant frequencies respectively. The larger the C_m, the higher the K_E, which implies stronger coupling or smaller external quality factor Q_E of the resonator [16]. Therefore, besides using the J-inverter network, C_m can also be easily checked for evaluating the magnitude of the coupling strength, which is more convenient for filter designers. The capacitance value can be calculated from the simulated Y-parameter data using Zeland *IE3D* as:

$$C_m = \mathrm{Im}(-Y_{21})/\omega. \tag{4.5}$$

Fig. 4.6 shows the comparison of the mutual capacitances C_m between two branches of both traditional and proposed ring filters. The proposed ring filter provides a relatively larger $\mathrm{I_m}$ ($-Y_{21}$) in the frequency range 5~9 GHz, thus achieves a larger mutual capacitance C_m and consequently a stronger coupling strength, which is consistent with the conclusion by means of the J-inverter network shown in Fig. 4.4.

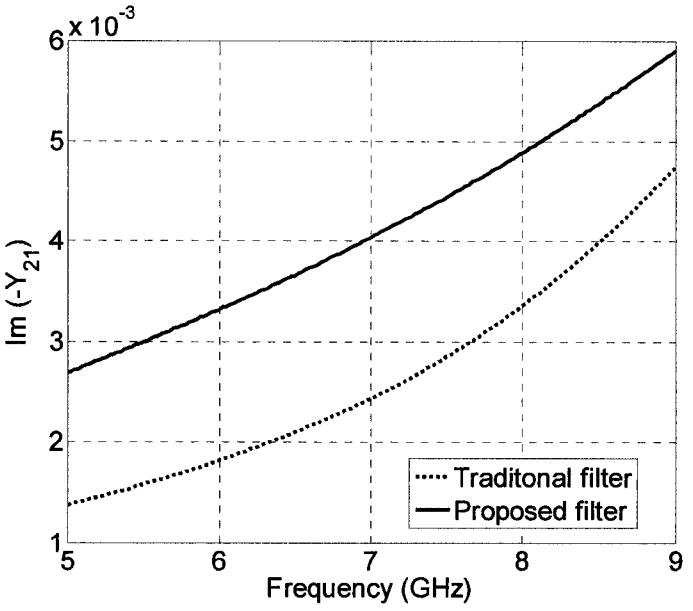

Fig. 4.6. Comparison of simulated susceptance of *Y*-parameter of the proposed filter and the traditional filter.

4.4 Salient Features of the Proposed Filter

4.4.1 Bandwidth Modulation

Bandwidth-efficient modulation techniques can enhance bandwidth efficiency while retaining reasonable power efficiency and implementation complexity/simplicity, thereby maximizing the use of available frequency spectrum of terrestrial and space-based communication systems. The interdigital capacitor is a multi-finger periodic structure, which uses the capacitance that occurs across a narrow gap between thin conductors. The capacitance C_{int} of an interdigital capacitor of length l_c can be expressed as [32]

$$C_{\text{int}} = (\varepsilon_r + 1) l_c \left[(N-3) A_1 + A_2 \right], \tag{4.6}$$

where

$$A_1 = 4.409 \tanh\left[0.55 (h/w_c)^{0.45} \right] \times 10^{-6} \tag{4.7}$$

and

$$A_2 = 9.92 \tanh\left[0.52 (h/w_c)^{0.5} \right] \times 10^{-6}. \tag{4.8}$$

In (4.6) through (4.8), ε_r and h are the dielectric constant and thickness of the substrate, N and w_c represent number and width of fingers of an interdigital capacitor respectively. By adjusting N (or other related parameters of interdigital capacitor), C_{int} can be altered. Since such capacitors are an integral part of the proposed filter, the bandwidths of the filter can be effectively adjusted by the interdigital capacitors. *IE3D* simulations of the proposed filter with different values of N are performed and the results are illustrated in Fig. 4.7. The bandwidths of proposed filters keep widening with the increase of N, while keeping f_0 fixed by slightly decreasing the lengths of the hairpin resonators. A summary of the simulation results is presented in Table 4.1. It can be observed that the bandwidth increases with N, while f_0 and locations of transmission zeros remain more or less unchanged. Changing N from 0 (*i.e.* traditional gap) to 8 lead to an increase in 3dB fractional bandwidth (*FBW*) from 5.8% to 15.5%, and a change in Q_E from 34.7 to 12.9, thus indicating a considerable degree of design flexibility for the designer/user. However, It must be pointed out that it may be difficult to design a filter with a *FBW* >20% using the proposed structure, since all the elements (e.g. line resonators, coupling elements) are highly dependent on frequency [33].

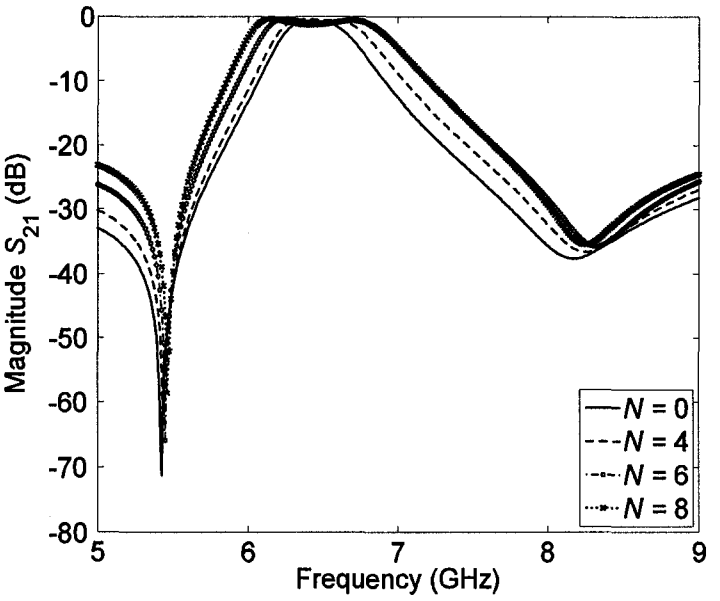

Fig. 4.7. *S*-parameters (S_{21}) of the proposed bandpass filter structure for different values of *N*.

TABLE 4.1
SUMMARY OF *IE3D* SIMULATIONS FOR DIFFERENT VALUES OF *N*

Number of Fingers	**0**	**4**	**6**	**8**
3dB Bandwidth	375MHz	602MHz	841MHz	1,005MHz
3dB *FBW*	5.8%	9.3%	12.9%	15.5%
Q_E	34.7	21.6	15.5	12.9
Dimension (mm^2)	5.3×6.0	4.9×6.4	4.1×7.2	3.45×8.0
Transmission Zeros	5.43GHz 8.19GHz	5.44GHz 8.25GHz	5.45GHz 8.31GHz	5.45GHz 8.25GHz

Recently, a ground plane aperture technique has been proposed [34] for effective enhancement of EM coupling over a wider frequency range. Based on this technique, two rectangular slots are etched in the ground plane below the two 4-finger interdigital capacitors as shown in Fig. 4.8(a) to further improve the bandwidth. Simulation results in Fig. 4.8(b) show that, increasing the width (T) of the ground plane apertures from 1.9 mm to 3.3 mm while keeping all other parameters unchanged, results in an increase in 3 dB *FBW* from 17.4% to 22.3%, and a change in Q_E from 11.5 to 8.8. It is to be noted that increasing T also results in a slight decrease in the lower cutoff frequency, an increase in the upper cutoff frequency, and a corresponding shift in the locations of the transmission zeros. The shift, *i.e.* an increase in f_0, can be countered by slightly increasing N alone. In essence, the proposed filters with etched slots offer flexibility in terms of broadband filter design.

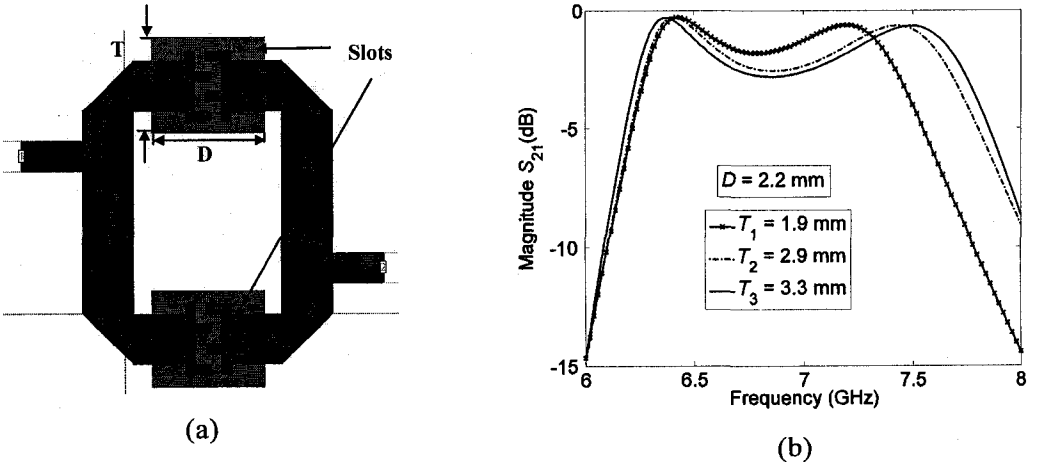

Fig. 4.8. (a) Layout of the proposed filter with etched ground plane apertures and (b) its simulated S_{21} for different values of T.

4.4.2 Transmission Zeros

In this section, consolidated formulations which help the estimation of transmission zeros of the proposed filter of Fig. 4.5(b), are presented. As can be seen in Fig. 4.5(b), the filter uses two hairpin resonators with asymmetric feed lines tapping the resonators. The input and the output feed lines divide the resonators into two sections of lengths l_1 and l_2 respectively. Coupling between the two resonators is approximated to be C_{int}, *i.e.*, the interdigital capacitance. Consequently, the entire circuit of Fig. 4.5(b) can be treated as a shunt circuit consisting of upper and lower sections. Each section is made up of l_1, C_{int} and l_2. The *ABCD* matrixes of the upper and the lower sections of the lossless shunt circuit can be expressed as

$$M_{upper} = \begin{pmatrix} A & B \\ C & D \end{pmatrix}_{upper} = M_1 M_2 M_3 \tag{4.9}$$

and

$$M_{lower} = \begin{pmatrix} A & B \\ C & D \end{pmatrix}_{lower} = M_3 M_2 M_1, \tag{4.10}$$

where

$$M_1 = \begin{pmatrix} \cos\beta(l_1 + \Delta l) & jz_0 \sin\beta l_1 (l_1 + \Delta l) \\ jy_0 \sin\beta(l_1 + \Delta l) & \cos\beta l_1 (l_1 + \Delta l) \end{pmatrix}, \tag{4.11}$$

$$M_2 = \begin{pmatrix} 1 & z_c \\ 0 & 1 \end{pmatrix}, \tag{4.12}$$

and

$$M_3 = \begin{pmatrix} \cos\beta(l_2+\Delta l) & jz_0 \sin\beta(l_2+\Delta l) \\ jy_0 \sin\beta(l_2+\Delta l) & \cos\beta l_2(l_2+\Delta l) \end{pmatrix}. \tag{4.13}$$

In (4.11) through (4.13), β is the propagation constant, $z_0 = 1/y_0$ is the characteristic impedance of each resonator, Δl accounts for the additional length of the microstrip in the interdigital capacitors, and $z_c = 1/j\omega C_{int}$ is the impedance of C_{int}.

The *ABCD* parameters are transformed into *Y*-parameters. The *Y*-parameters of the upper and lower sections are given by

$$\begin{pmatrix} Y_{11} & Y_{12} \\ Y_{21} & Y_{22} \end{pmatrix}_i = \begin{pmatrix} D_i/B_i & (B_iC_i - A_iD_i)/B_i \\ -1/B_i & A_i/B_i \end{pmatrix}, \tag{4.14}$$

where i = either *upper* or *lower* accordingly. The *Y*-parameters of the entire shunt circuit/structure can be obtained by adding those of the upper and the lower sections *i.e.*

$$\begin{pmatrix} Y_{11} & Y_{12} \\ Y_{21} & Y_{22} \end{pmatrix} = \begin{pmatrix} Y_{11} & Y_{12} \\ Y_{21} & Y_{22} \end{pmatrix}_{upper} + \begin{pmatrix} Y_{11} & Y_{12} \\ Y_{21} & Y_{22} \end{pmatrix}_{lower}. \tag{4.15}$$

From the above *Y*-parameters, S_{21} of the filter circuit can be calculated. For instance, the numerator of S_{21} is given by

$$S_{21(numerator)} = -j4\{z_0 \sin[\beta(l_1+\Delta l)+\beta(l_2+\Delta l)] - \frac{\cos\beta(l_1+\Delta l)\cos\beta(l_2+\Delta l)}{\omega C_{\text{int.}}}\}. \tag{4.16}$$

Transmission zeros of the proposed filter can then be estimated by setting (4.16) to 0, *i.e.*

$$z_0 \sin[\beta(l_1+\Delta l)+\beta(l_2+\Delta l)] - \frac{\cos\beta(l_1+\Delta l)\cos\beta(l_2+\Delta l)}{\omega C_{\text{int.}}} = 0. \tag{4.17}$$

In addition, assuming C_{int} to be small leads to

$$\cos\beta(l_1+\Delta l)\cos\beta(l_2+\Delta l)\approx 0\,, \tag{4.18}$$

which relates the transmission zeros to the tapping positions. Substituting β in (4.18) by $2\pi f\sqrt{\varepsilon_{eff}}/c$ yields estimated locations of the transmission zeros *i.e.*

$$f_1=\frac{c}{4(l_1+\Delta l)\sqrt{\varepsilon_{eff}}} \tag{4.19}$$

and

$$f_2=\frac{c}{4(l_2+\Delta l)\sqrt{\varepsilon_{eff}}}\,, \tag{4.20}$$

where f is the frequency, ε_{eff} is the effective dielectric constant, c is the speed of light in the free space, and f_1 and f_2 are the frequencies of the two transmission zeros corresponding to the tapping positions of the lengths of $l_1$and l_2 on the resonators. For simplifying the computation of f_1 and f_2, Δl is eliminated by introducing two new linear coefficients $\{P_1, P_2\} \in (0, 1)$ leading to new simplified expressions *i.e.*

$$f_1=\frac{P_1 c}{4l_1\sqrt{\varepsilon_{eff}}} \tag{4.21}$$

and

$$f_2=\frac{P_2 c}{4l_2\sqrt{\varepsilon_{eff}}}\,. \tag{4.22}$$

From (4.21) and (4.22), it can be stated that the locations of the transmission zeros (f_1 and f_2) can be controlled by the positions of tapping lines (l_1 and l_2) and/or by the linear coefficients (P_1 and P_2, which relate to the geometry of the interdigital capacitors).

In order to determine f_1 and f_2, EM simulations are performed in Zeland *IE3D* to first evaluate P_1 and P_2 for filters with different interdigital capacitors (*i.e.* capacitors with varying number of figures N). Since the capacitance C_{int} varies proportionally with N, the branch lengths of the hairpin resonators need to be slightly adjusted for keeping the center frequency f_0 fixed while changing N. Based on the simulations, a set of empirical values for P_1 and P_2 are reported in Table I, applicable to the proposed filter structures. Both P_1 and P_2 decrease with increasing N. This is expected since the more the fingers, the more the extra microstrip length Δl. In essence, (4.21) and (4.22) based on linear coefficients offers accurate estimations of the transmission zeros with relative errors below 6.5%. To confirm this, several 4-finger ring bandpass filters with different tapping positions are designed at f_0 = 6.5 GHz. The locations of their transmission zeros as predicted by the proposed model (4.21) and (4.22) are compared with those from Zeland *IE3D* simulations. Such comparisons are presented in Table II. For the case of $N = 4$, the maximum relative error between the proposed model and the EM simulations is 3.8%.

As can be seen in Fig. 4.10, the shorter the distance from the centre of the hairpins to the input/output ports, the closer the two transmission zeros are to the passband, consequently providing a high selectivity. However, it has to be noted that the tapping positions also affect the coupling between the resonators. The closer the tapping positions

TABLE 4.2

EMPIRICAL VALUES OF P_1 AND P_2 FOR THE PROPOSED FILTERS WITH DIFFERENT N

Number of Fingers	P_1	P_2	Relative Error
2 fingers	0.7754	0.8232	< 6.4%
3 fingers	0.7531	0.7947	< 5.0%
4 fingers	0.7243	0.7566	< 3.8%
5 fingers	0.6862	0.7055	< 3.2%
6 fingers	0.6455	0.6520	< 4.2%
7 fingers	0.6134	0.6104	< 5.1%
8 fingers	0.5853	0.5740	< 3.9%
9 fingers	0.5633	0.5469	< 5.7%

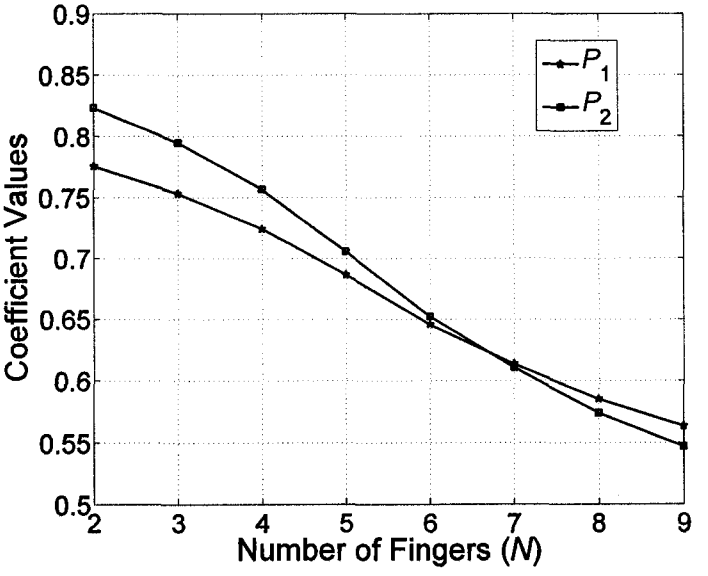

Fig. 4.9. Empirical values of linear coefficients P_1 and P_2 for the proposed bandpass filters with different N.

are to the center of the hairpins, the larger the Q_E [16]. A large Q_E puts the filter into an over-coupled situation [35][36] *i.e.*

$$K > \frac{1}{Q_u} + \frac{1}{Q_E}, \tag{4.23}$$

where K is the coupling coefficient and Q_u is the unloaded quality factor of either of the two resonators. For instance, the case of l_1 = 2.8 mm and l_2 = 3.6 mm in Fig. 4.10 reflects an over-coupled situation causing a hump within the passband. The coupling condition of the filter can be identified by using either measured or simulated values of K, Q_u and Q_E [37]-[39]. While Q_E and K can be calculated using equations (4.3) and (4.4), an expression for Q_u is available in [39]. In the case of the proposed filter of Fig. 4.5 (b) with N = 4, K = 0.03 < $1/Q_u$ + $1/Q_E$ = 1/78.9 + 1/25, thereby satisfying the under-coupled condition, and the filter response does not show a hump in the passband. The coupling gap S_{int} between the interdigital capacitors also affects the EM coupling between two resonators [39]. In the case of the proposed filter of Fig. 4.5 (b), S_{int} = 0.2 mm, set by the trial-and-error simulations for the optimal frequency response. In essence, both the tapping positions and the gap size must be carefully chosen in order to avoid over-coupling.

TABLE 4.3
SIMULATED AND ESTIMATED TRANSMISSION ZEROS FOR BANDPASS FILTERS WITH $N = 4$ AND DIFFERENT TAPPING POSITIONS

Tapping Positions	**IE3D Simulation**	**Proposed Estimation**	**Relative Error**
l_1 = **2.4mm**	f_1=8.25GHz	f_1=8.49GHz	E_1=**2.9%**
l_2 = **4.0mm**	f_2=5.45GHz	f_2=5.32GHz	E_2=**2.4%**
l_1 = **2.6mm**	f_1=7.85GHz	f_1=7.84GHz	E_1=**0.1%**
l_2 = **3.8mm**	f_2=5.58GHz	f_2=5.60GHz	E_2=**0.4%**
l_1 = **2.8mm**	f_1=7.49GHz	f_1=7.28GHz	E_1=**2.8%**
l_2 = **3.6mm**	f_2=5.77GHz	f_2=5.91GHz	E_2=**3.8%**
l_1 = **3.2mm**	No passband	f_1=6.37GHz	*NA*
l_2 = **3.2mm**		f_2=6.65GHz	

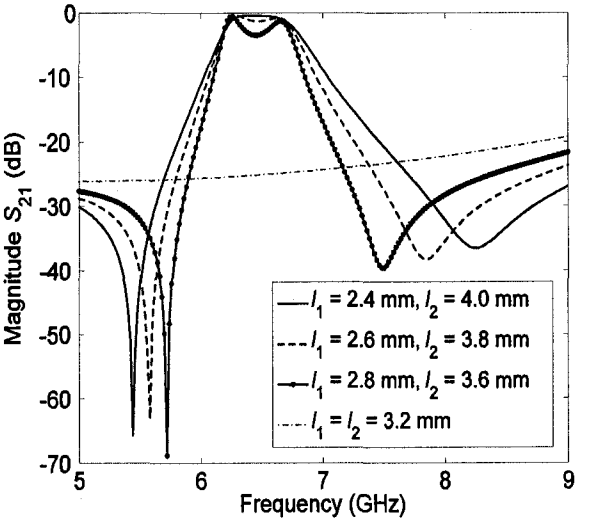

Fig. 4.10. Simulated *S*-parameters (S_{21}) of the proposed bandpass filters with $N = 4$ and different tapping positions.

4.4.3 Cascaded Structures

In general, relatively sharper frequency responses and flatter passband can be achieved by cascaded bandpass filter structures. Consider given user-specifications of a filter, such as maximum passband attenuation = 2 dB, minimum stopband attenuation = 30 dB, maximum return loss = -15 dB, f_0 = 6.5 GHz, 3 dB bandwidth ≈ 650 MHz, and transmission zeros at 5.5 GHz and 8.3 GHz respectively. Such specifications are difficult to achieve using a single unit, and cascading becomes necessary. Based on these specifications, two filter units both with N = 4 are selected in the design of cascaded filters. Since the transmission zeros of the cascaded filter are required to be at 5.5 GHz and 8.3 GHz, equations (4.21) and (4.22), and coefficients P_1 = 0.7243 and P_2 = 0.7566 of Table I are used, leading to tapping line positions l_1 = 2.43 mm and l_2 = 4.01 mm.

The first of the two cascaded filters (see Fig. 4.11(a)) is implemented by directly coupling two identical interdigital ring units. In order to obtain lower RL and sharper cutoff frequency response, D = 2.68 mm is chosen for vertical offset of the two cascaded units, and S = 0.522 mm for the horizontal coupling gap between the units by simulation and optimization. Based on (4.3) and (4.4), the external quality factor Q_E is calculated to be 19.1 and the coupling matrix M is found to be

$$M = \begin{bmatrix} M_{11} & M_{12} & M_{13} & M_{14} \\ M_{21} & M_{22} & M_{23} & M_{24} \\ M_{31} & M_{32} & M_{33} & M_{34} \\ M_{41} & M_{42} & M_{43} & M_{44} \end{bmatrix} = \begin{bmatrix} 0 & -0.038 & 0 & 0 \\ -0.038 & 0 & 0.029 & 0 \\ 0 & 0.029 & 0 & -0.043 \\ 0 & 0 & -0.043 & 0 \end{bmatrix}, \quad (4.24)$$

where $M_{i,j} = \left(\frac{f_{r2}^{\,2} - f_{r1}^{\,2}}{f_{r2}^{\,2} + f_{r1}^{\,2}} \right)_{i,j}$ is the mutual coupling between the ith resonator and jth resonator, $(f_{r1})_{i,j}$ and $(f_{r2})_{i,j}$ are the lower and higher resonant frequencies of the ith resonator and jth resonator. Negative and the positive values in M represent electric and magnetic couplings respectively [16].

An alternative cascaded structure is shown in Fig. 4.12(a). In this case, a double stub microstrip is used to adjust the impendence matching between the two cascaded units. Because of the added microstrip, the transmission zeros of the cascaded filter are expected to shift from the estimated values. The external quality factor Q_E is calculated to be 22.1 and the coupling matrix M is found to be

$$M = \begin{bmatrix} 0 & -0.042 & 0 & 0 \\ -0.042 & 0 & 0.820 & 0 \\ 0 & 0.820 & 0 & -0.048 \\ 0 & 0 & -0.048 & 0 \end{bmatrix}. \tag{4.25}$$

Both of the cascaded filters have met the design specifications. Compared to the cascaded filter of Fig. 4.11, the filter of Fig. 4.12 exhibits a relatively larger Q_E, a lower insertion loss, and a sharper cutoff frequency response. As such, the filter of Fig. 4.12 has better frequency selectivity, although it is relatively bulky.

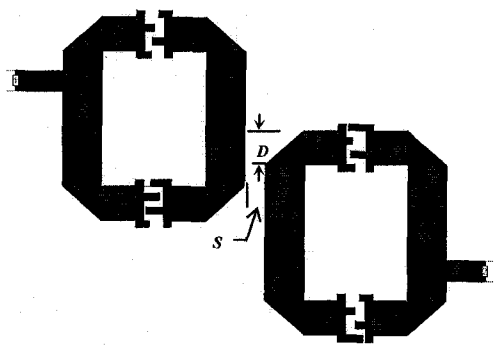

(a)

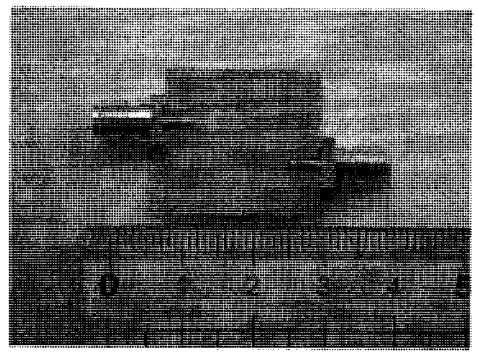

(b)

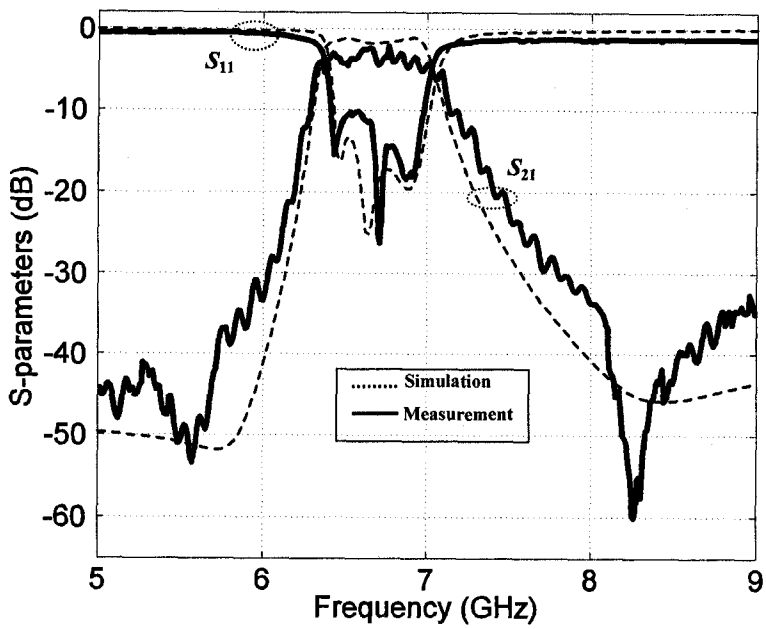

(c)

Fig. 4.11. (a~b) Layout of a cascaded coupling bandpass filter based on the proposed filter and (c) its simulated and measured *S*-parameters.

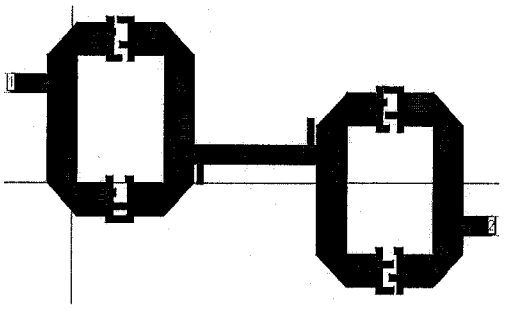

(a)

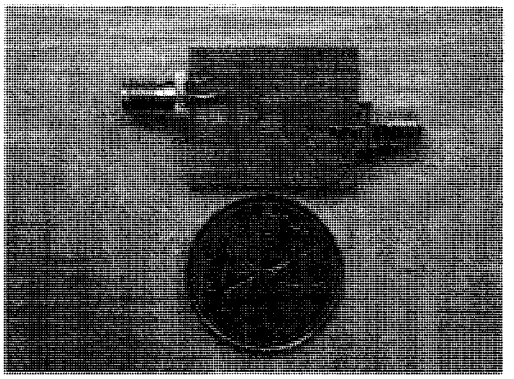

(b)

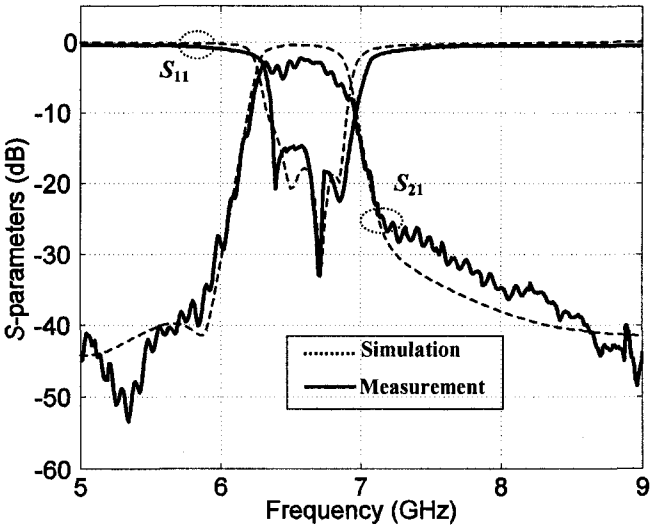

(c)

Fig. 4.12. (a~b) Layout of another cascaded coupling bandpass filter based on the proposed filter and (c) its simulated and measured *S*-parameters.

4.4.4 Fabrication and Measurement

The proposed bandpass filters are fabricated on a 0.635 mm thick RT/duroid 6010.2 substrate with ε_r = 10.2. Measurements are performed using an Anritsu 37369D vector network analyzer. Fig. 4.13(b) shows the measured and simulated *S*-parameters of the fabricated 8-finger bandpass filter of Fig. 4.13(a). The filter shows a centre frequency of 6.5 GHz and a 3dB bandwidth of 1018 MHz, both of which agree with the *IE3D* simulations. The filter has a return loss greater than 15 dB over the passband ranging from 6.48 GHz to 6.91 GHz and an insertion loss greater than 2 dB within the 6.3-6.88 GHz range. Maximum group delay variation within the passband is 0.23 ns (see Fig. 4.13(c)). Fig. 4.14(a) shows the measured and simulated *S*-parameters of the fabricated filters with etched ground plane for the case of T = 3.3 mm (see Fig. 4.14(b)). The filter shows a 3 dB *FBW* of 24.2%. The filter has a return loss above 15 dB over the passband, ranging from 6.81 GHz to 7.82 GHz, and an insertion loss greater than 2 dB within the 6.51-7.85 GHz range.

Both the simulations and experimental measurements of cascaded structures are shown in Fig. 4.11(c) and Fig. 4.12(c) respectively. Regardless of some small deviation in the higher frequency, satisfactory agreement between the simulation and the measured responses is achieved. Fig. 4.15 shows a group of 4-finger bandpass filters designed and fabricated with different tapping positions. These filters exhibit different transmission zeros as expected.

Discrepancies between measurements and simulations can be attributed to fabrication tolerances, considering the high sensitivity of ring resonators with respect to dielectric

constant and thickness of the substrate [40], and to some extent to calibration errors. In addition, the undesirable effects of radiation from discontinuities (fingers in particular) in the proposed filters tend to be also the cause for the minor deterioration of the insertion loss [41].

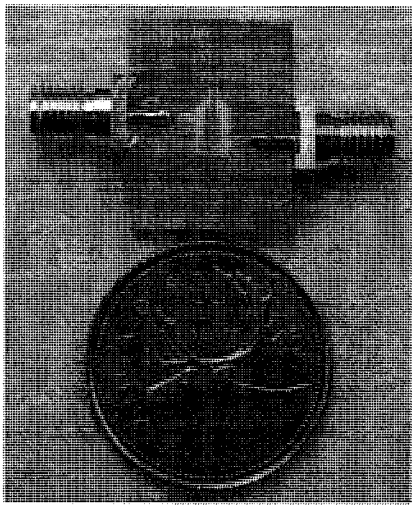

(a)

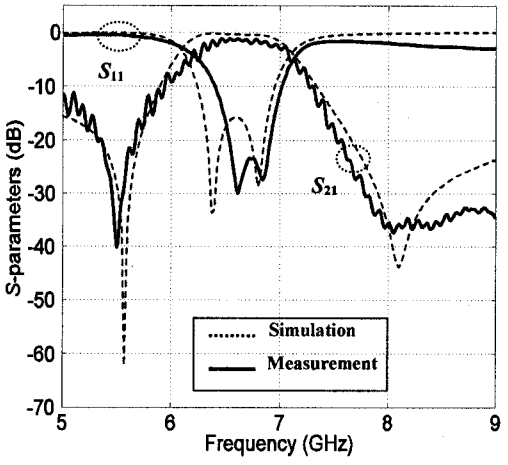

(b)

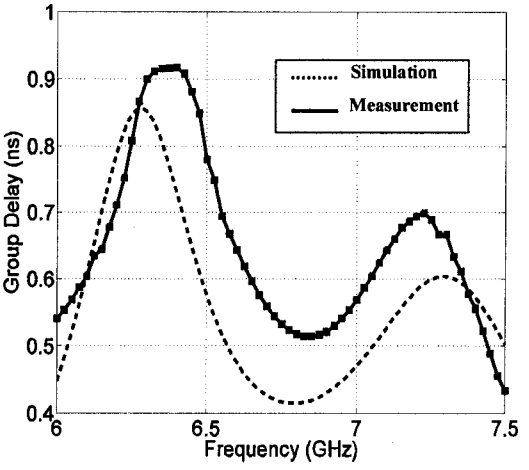

(c)

Fig. 4.13. (a) Photograph of an 8-finger bandpass filter, (b) its simulated and measured *S*-parameters, (c) its simulated and measured group delay.

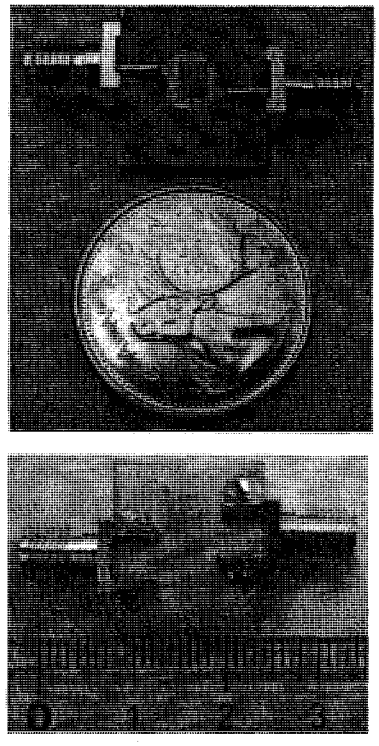

(a)

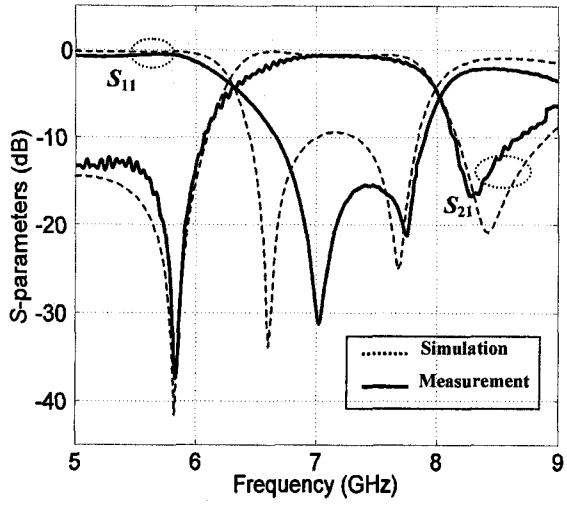

(b)

Fig. 4.14. (a) Photographs of top view and bottom view of a 4-finger bandpass filter with etched ground planes, and (b) its simulated and measured *S*-parameters.

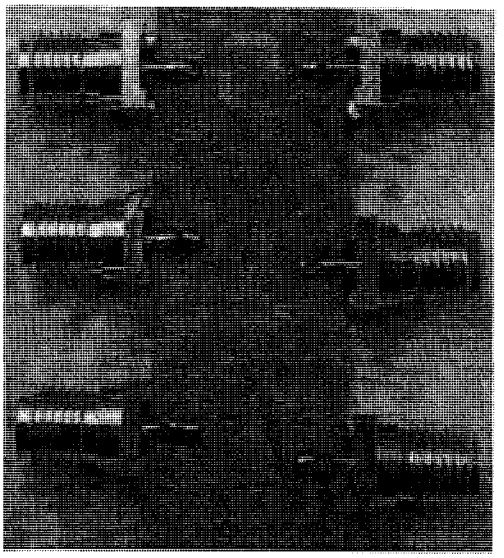

(a)

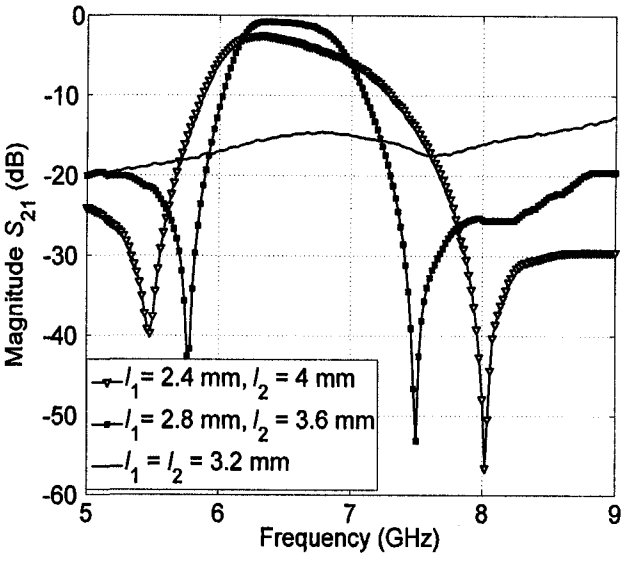

(b)

Fig. 4.15. (a) Photograph of a group of bandpass filters with $N = 4$ and with different tapping positions, and (b) their measured S-parameters.

4.5 Summary

In this chapter, a class of new microstrip ring bandpass filters, which overcomes the typical fabrication limitation of traditional ring filters, has been proposed. The proposed filters use interdigital capacitors combined with ring resonators, and exhibit a much wider bandwidth compared to traditional edge-coupled filters. The bandwidth of the filters can be easily adjusted by changing the geometrical parameters of the interdigital capacitors and/or the ground plane apertures. The filters can be employed in both narrowband ($FBW < 20\%$) and wideband ($FBW > 20\%$) commutation circuits. Semi-analytical equations derived in this work help designers quickly yet accurately estimate the locations of transmission zeros. Further, cascaded filters based on the proposed structure exhibit a very sharp cutoff frequency and low loss. Both measurement and simulation results have been shown for several filters. This research can be useful for improvising computer aided filter design packages/tools.

Chapter 5

Conclusions

Microwave printed filters provide various advantages over waveguide and coaxial line filters, such as low weight, low cost, compact size and high accuracy, which benefits modern mobile and satellite communication systems. In such communication systems, volume of printed filters involved is always required to be miniaturized to facilitate circuit integration. Broader bandwidths are also desirable for better information capacity. Such requirements lead to critical challenges in design and implementation of the filters. In order to meet these requirements, the work in this thesis has focused on two aspects. First, a very compact and low loss printed bandpass filter has been implemented. Second, a technique to effectively increase the bandwidth of printed filters without going beyond fabrication limitations has been developed.

CRLH-TL is promising in terms of volume minimization of microwave circuits due to the negative and nonlinear nature of phase constant (β) versus frequency. A simple CRLH-TL structure has been proposed using a microstrip interdigital capacitor whose outer arms are grounded by vias. Based on the CRLH structure, a new bandpass filter has

been designed. The simulation results of the CRLH filter shows a minimum insertion loss of 0.33 dB and a wide 3-dB fractional bandwidth of 49.4%. Moreover, the volume of the proposed CRLH filter (4.23×1.5 mm^2) is about 10 times smaller than traditional printed filters with a comparable frequency response. In addition, a geometrical parameter analysis of the CRLH filter has been undertaken. This analysis has lead to the development of an automated design algorithm for CRLH filters. The proposed algorithm has been validated through a practical example.

In the design of printed filters, a wider bandwidth can normally be achieved by improving EM coupling between resonators. This can be implemented by reducing gap and/or strip widths of the resonators. However, such an approach leads to a lower quality factor Q and higher insertion loss. Furthermore, effectiveness of the approach may be affected by geometric limitations in typical fabrication processes, such as a minimum gap/strip width of 0.13 mm. In order to overcome such limitations, a set of new microstrip bandpass filters using interdigital capacitors combined with ring resonators has been proposed in the thesis. The proposed filters exhibit 2 to 3 times wider bandwidths compared to traditional ring filters. Furthermore, the bandwidth of the filter can be easily adjusted by changing the geometrical parameters of the interdigital capacitors and/or the ground plane apertures. The filters can be employed in both narrowband ($FBW < 20\%$) and wideband ($FBW > 20\%$) communication circuits. Semi-analytical equations which can quickly yet accurately estimate the locations of transmission zeros have been derived in this work with a maximum relative error of 6.4 %. Finally, cascaded filters based on the proposed structure exhibit a very sharp cutoff frequency and low loss.

Several filters have been fabricated and tested using a vector network analyzer. Measured frequency responses of the proposed filters have shown a wide adjustable bandwidth from 375 MHz to 1560 MHz. These results are in good agreement with those simulated using Zeland *IE3D* in the 5-9 GHz range.

The work presented in this thesis, namely the development of the CRLH and interdigital ring filters, provides an effective solution to the problems of manufacturing limitations of geometric size and helps to facilitate the design of filters. CRLH filters can also be applied in time-domain applications, *e.g.* delay-lines. Compact CRLH delay lines offer longer delay compared to traditional RH microstrip delay lines, and the delay can be tuned by adjusting the geometrical parameters of the interdigital capacitors. The proposed ring resonator filters can potentially be combined with a piezoelectric transducer (PET) and an attached dielectric perturber to allow for a tunable center frequency. Thus, coupled with the bandwidth adjustability provided by the proposed filter structure, the future ring filters can offer even greater design flexibility for the RF/Microwave designer.

References

[1] F. Sterzer, "Microwave medical devices", *IEEE Microwave Magazine*, vol. 3, pp. 65–70, 2002.

[2] N.M. Nedeltchev, P.J. Claude, and H. Baudrand, "Microwave Scattering from Stratified Heterogeneous Random Medium Embedded with Non-Spherical Particles", *Proc. EuMC*, London, UK, Sept. 1999, pp. 165–168.

[3] F. Ivanek, "50 Years of Microwave Communications Systems Development in the San Francisco Bay Area", *Proc. IEEE MTT-S Int. Symp.*, San Francisco, CA, June 2006, pp. 996–999.

[4] "Breakthrough of the year: The runners-up," *Science*, vol. 302, pp. 2039–2045, 2003.

[5] V. Veselago, "The electrodynamics of substances with simultaneously negative values of ε and μ", *Soviet Physics Uspekhi*, vol. 10, pp. 509–514, 1968.

[6] S. Ramo, J.R. Whinnery, and T. Van Duzer, *Fields and Waves in Communication Electronics*, New York, NY: John Wiley, 1984.

[7] R.A. Shelby, D.R. Smith, and S. Schultz, "Experimental verification of a negative index of refraction," *Science*, vol. 292, pp. 77–79, 2001.

[8] C. Caloz, H. Okabe, T. Iwai, and T. Itoh, "Transmission line approach of left-handed (LH) materials," in *Proc. USNC/URSI National Radio Science Meeting*, San Antonio, TX, June 2002, p. 39.

[9] G.V. Eleftheriades, O. Siddiqui, and A.K. Iyer, "Transmission line models for negative refractive index media and associated implementations without excess resonators," *IEEE Microwave Wireless Compon. Lett.*, vol. 13, pp. 51–53, Feb. 2003.

[10] Y. Shen and R.R. Mansour, "An innovative CAD technique for microstrip filter design," *IEEE Tran. Microwave Theory and Tech.*, vol. 45, pp. 780–786, 1997.

[11] C.P. Dong, G.L. Matthaei, and S.W. Mu, "Bandstop Filter Design Using a Dielectric Waveguide Grating" *IEEE Tran. Microwave Theory and Tech.*, vol. 33, pp. 693–702, 1985.

[12] W.A. Davis and P.J. Khan, "Coaxial Bandpass Filter Design", *IEEE Tran. Microwave Theory and Tech.*, vol. 19, pp. 373–380, 1971.

[13] I.H. Zabalawi, "Microwave printed circuit linear phase selective filter design", *Proc. IEEE*, vol. 70, pp. 767–769, 1982.

[14] E.L. Holzman, "Wideband measurement of the dielectric constant of an FR4 substrate using a parallel-coupled microstrip resonator", *IEEE Tran. Microwave Theory and Tech.*, vol. 54, pp. 3127–3130, 2006.

[15] L.K. Yeung and K.-L. Wu, "A Dual-Band Coupled-Line Balun Filter", *IEEE Tran. Microwave Theory and Tech.*, vol. 55, pp. 2406–2411, 2007.

[16] J.S. Hong and M.J. Lancaster, *Microstrip Filters for RF/Microwave Applications*, New York, NY: John Wiley & Sons, 2001.

[17] C. Caloz, A. Sanada, L. Liu, and T. Itoh, "A broadband left-handed (LH) coupled-line backward coupler with arbitrary coupling levels," in *Proc. IEEE MTT-S Int. Symp.*, Philadelphia, PA, June 2003, pp. 317–320.

[18] I. Lin, C. Caloz, and T. Itoh, "A branch line coupler with two arbitrary operating frequencies using left-handed transmission lines," in *Proc. IEEE MTT-S Int. Symp.*, Philadelphia, PA, June 2003, pp.325–327.

[19] H. Okabe, C. Caloz, and T. Itoh, "A compact enhanced hybrid ring using a left-handed transmission line section," in *Proc. IEEE MTT-S Int. Symp.*, Philadelphia, PA, June 2003, pp. 329–332.

[20] A. Grbic and G. V. Eleftheriades, "A backward-wave antenna based on negative refractive index," in *Proc. IEEE AP-S Int. Symp.*, San Antonio, TX, June 2002, pp. 340–343.

[21] L. Zhu, Q. Zhu, C. Chen, and J. Zhang, "Bandpass filter with micro-strip LH transmission line structure," *Proc. APMC*, New Delhi, India, Dec. 2004.

[22] P. Troughton, "Measurement techniques in microstrip," *Electronics Letters*, vol. 5, pp. 25–26, 1969.

[23] Lei Zhu and K. Wu, "Line-to-ring coupling circuit model and its parametric effects for optimized design of microstrip ring circuits and antennas", *Proc. IEEE MTT-S Int. Symp.*, Denver, CO., June, 1997, pp. 289–292.

[24] S. Sun and Lei Zhu, "Wideband microstrip ring resonator bandpass filters under multiple resonances", *IEEE Tran. Microwave Theory and Tech.*, vol. 55, pp. 2176–2182, 2007.

[25] J.-C. Chien and L.-H. Lu, "Analysis and design of wideband injection-locked ring oscillators with multiple-input injection", *IEEE Journal of Solid-State Circuits*, vol. 42, pp. 1906–1915, 2007.

[26] A. Lai, T. Itoh, and C. Caloz, "Composite right/left-handed transmission line metamaterial", *IEEE Microwave Magazine*, vol. 5, pp. 34–50, 2004.

[27] S.Y. Lee and C.M. Tsai, "New cross-coupled filter design using improved hairpin resonators", *IEEE Trans. Microwave Theory Tech.*, vol. 48, pp. 2482–2490, 2000.

[28] L.H. Hsieh and K. Chang, "Tunable microstrip bandpass filters with two transmission zeros", *IEEE Trans. Microwave Theory Tech.*, vol. 51, pp. 520–525, 2003.

[29] Lei Zhu and K. Wu, "Characterization of unbounded multiport microstrip passive circuits using an explicit network-based method of moments", *IEEE Trans. Microwave Theory Tech.*, vol.45, pp. 2114–2124, 1997

[30] Lei Zhu and K. Wu, "Unified equivalent-circuit model of planar discontinuities suitable for field theory-based CAD and optimization of M(H)MIC," *IEEE Trans. Microwave Theory Tech.*, vol. 45, pp. 2114–2124, 1999.

[31] Lei Zhu and K. Wu, "Accurate circuit model of interdigital capacitor and its application to design of new quasi-lumped miniaturized filters with suppression of harmonic resonance," *IEEE Trans. Microwave Theory Tech.*, vol. 48, pp. 347–356, 2000.

[32] I.J. Bahl, *Lumped Elements for RF and Microwave Circuits*, Norwood, MA: Artech House, 2003.

[33] Lei Zhu, H. Bu, and K. Wu, "Broadband and compact multi-pole microstrip bandpass filters using ground plane aperture technique," *IEE Proc. Microwaves Antennas Propagat.*, vol. 149, pp. 71–77, 2002.

[34] Lei Zhu, H. Bu, and K. Wu, "Multilayered coupled-microstrip lines technique with aperture compensation for innovative planar filter design", *Proc. APMC*, Singapore, Nov. 1999, pp. 303–306.

[35] G.L. Matthaei, L. Young, and E.M.T. Jones, *Microwave Filters, Impedance-Matching Networks, and Coupling Structures*, New York, NY: McGraw-Hill, 1980.

[36] L.-H. Hsieh and K. Chang, "Dual-mode quasi-elliptic-function bandpass filters using ring resonators with enhanced-coupling tuning stubs," *IEEE Trans. Microwave Theory Tech.*, vol. 50, pp. 1340–1345, 2002.

[37] J.-S. Hong and M.J. Lancaster, "Couplings of microstrip square open-loop resonators for cross-coupling planar microwave filters," *IEEE Trans. Microwave Theory Tech.*, vol. 44, pp. 2099–2109, 1996.

[38] R.S. Kwok and J.F. Liang, "Characterization of high-Q resonators for microwave-filter applications," *IEEE Trans. Microwave Theory Tech.*, vol. 47, pp. 111–114, 1999.

[39] K. Chang, *Microwave Ring Circuits and Antennas*, New York, NY: John Wiley & Sons, 1996.

[40] K. Chang and L.H. Hsieh, *Microwave Ring Circuits and Related Structures*, Hoboken, NJ: John Wiley & Sons, 2004.

[41] P.B. Katehi and L.P. Dunleavy, "Microstrip filter design including dispersion effects and radiation losses," *Proc. IEEE MTT-S Int. Microwave Symp.*, Baltimore, MD, June 1986, pp. 687-690.

Publications related to the work of the thesis

[42] L. Zhu, V. K. Devabhaktuni, and C. Wang, "CAD of left-handed transmission line bandpass filters," *Proc. Progress in Electromagnetics Research Symp.*, Beijing, China, March 2007, pp. 77–82.

[43] S. Sebak, L. Zhu, V. K. Devabhaktuni, and C. Wang, "CRLH microstrip delay Line for high-speed electronic circuits," *Proc. Progress in Electromagnetics Research Symp.*, Beijing, China, March 2007, pp. 259-263.

[44] L. Zhu, V. K. Devabhaktuni, C. Wang and M. Yu, "Adjustable bandwidth filter design based on interdigital capacitors", *IEEE. Microwave and Wireless Component Lett.*, vol. 18, pp. 16–18, 2008.

[45] L. Zhu, V. K. Devabhaktuni, C. Wang and M. Yu, "Cascaded interdigital ring bandpass filters with predictable transmission zeros", *IEEE. Microwave and Wireless Component Lett.*, 2008. (pending)